Monthly Notices
of the
ROYAL ASTRONOMICAL SOCIETY

Mon. Not. R. Astron. Soc. **408,** 1628–1648 (2010) doi:10.1111/j.1365-2966.2010.17227.x

Keck spectroscopy of faint $3 < z < 7$ Lyman break galaxies – I. New constraints on cosmic reionization from the luminosity and redshift-dependent fraction of Lyman α emission

Daniel P. Stark,[1]★ Richard S. Ellis,[2] Kuenley Chiu,[2] Masami Ouchi[3]† and Andrew Bunker[4]

[1]*Kavli Institute of Cosmology & Institute of Astronomy, University of Cambridge, Madingley Road, Cambridge CB3 0HA*
[2]*California Institute of Technology, 1200 E. California Blvd. Pasadena, CA 91125, USA*
[3]*Observatories of the Carnegie Institution of Washington, 813 Santa Barbara Street Pasadena, CA 91101, USA*
[4]*Department of Physics, University of Oxford, Denys Wilkinson Building, Keble Road, Oxford OX1 3RH*

Accepted 2010 June 21. Received 2010 June 21; in original form 2010 April 1

ABSTRACT

We present the first results of a new Keck spectroscopic survey of UV faint Lyman break galaxies in the redshift range $3 < z < 7$. Combined with earlier Keck and published European Southern Observatory (ESO) VLT data, our spectroscopic sample contains more than 600 dropouts offering new insight into the nature of sub-L^* sources typical of those likely to dominate the cosmic reionization process. In this first paper, in a series discussing these observations, we characterize the fraction of strong Lyα emitters within the continuum-selected dropout population. By quantifying how the 'Lyα fraction', $x_{\rm Ly\alpha}$, varies with redshift, we seek to constrain changes in Lyα transmission associated with reionization. In order to distinguish the effects of reionization from other factors which affect the Lyα fraction [e.g. dust, interstellar medium (ISM) kinematics], we study the luminosity and redshift-dependence of the Lyα fraction over $3 \lesssim z \lesssim 6$, when the intergalactic medium (IGM) is known to be ionized. These results reveal that low-luminosity galaxies show strong Lyα emission much more frequently ($x_{\rm Ly\alpha} = 0.47 \pm 0.16$ at $M_{\rm UV} = -19$) than luminous systems ($x_{\rm Ly\alpha} = 0.08 \pm 0.02$ at $M_{\rm UV} = -21$), and that at fixed luminosity, the prevalence of strong Lyman α emission increases moderately with redshift over $3 < z < 6$ (d $x_{\rm Ly\alpha}$/d $z = 0.05 \pm 0.03$). Based on the bluer mean UV slopes of the strong Lyα emitting galaxies in our data set ($\langle\beta\rangle_{\rm Ly\alpha} - \langle\beta\rangle_{\rm no\,Ly\alpha} = -0.33 \pm 0.09$ at $M_{\rm UV} = -20.5$) we argue that the Lyα fraction trends are governed by redshift and luminosity-dependent variations in the dust obscuration, with likely additional contributions from trends in the kinematics and covering fraction of neutral hydrogen. Using the limited infrared spectroscopy of candidate $z \simeq 7$ galaxies, we find a tentative decrease in the Lyα fraction by a factor of >1.9 with respect to the predicted $z \simeq 7$ value, a result which, if confirmed with future surveys, would suggest an increase in the neutral fraction by this epoch. Given the abundant supply of z and Y drops now available from deep Hubble WFC3/IR surveys, we show it will soon be possible to significantly improve estimates of the Lyα fraction using optical and near-infrared multi-object spectrographs, thereby extending the study conducted in this paper to $7 \lesssim z \lesssim 8$.

Key words: galaxies: evolution – galaxies: formation – galaxies: high-redshift – cosmology: observations.

1 INTRODUCTION

Considerable observational progress has been achieved in recent years in the study of star-forming galaxies seen beyond $z \simeq 3$, a period corresponding to $\simeq 2$ Gyr after the big bang. It is now clear that this is a period of rapid galaxy evolution and a

★E-mail: dps@ast.cam.ac.uk
†Carnegie Fellow.

number of key results have emerged from recent multi-wavelength surveys.

For the colour-selected $z > 3$ Lyman break galaxies (LBGs), it is now established from various independent surveys that the star formation density, deduced from rest-frame UV luminosities, declines monotonically with redshift (e.g. Stanway, Bunker & McMahon 2003; Bunker et al. 2004) largely as a result of a corresponding fading of the characteristic UV luminosity (e.g. Ouchi et al. 2004; Yoshida et al. 2006; Bouwens et al. 2006, 2007; McLure et al. 2010). The associated stellar mass density in LBG, deduced from near-infrared *Spitzer* photometry, increases by $\simeq$1 dex from $z \simeq 6$ to 4 (Eyles et al. 2007; Stark et al. 2009). As the rate of change of stellar mass is governed by ongoing star formation, it is useful to relate the two measures and such a comparison indicates a rapid duty-cycle of star formation activity at this time, unlike the more continuous modes seen for equivalent sources at $z \simeq 2$–3 (Stark et al. 2009). By contrast, the redshift-dependent luminosity function (LF) of narrow-band selected *Lyman α emitters* (LAE) shows no equivalent decline with redshift over $3 < z < 6$ (Ouchi et al. 2008), suggesting an increasing fraction of line emitters amongst the star-forming population at early times. Moreover, detailed studies of the slope of the UV continuum in $z > 3$ LBGs indicate a decreasing dust content at earlier times (e.g. Stanway, McMahon & Bunker 2005; Bouwens et al. 2006, 2009b) as well as a luminosity dependence at $z \simeq 3$ (e.g. Reddy & Steidel 2009). Conceivably the combination of a reduced dust content and a shift to more intense, shorter-term star formation at high redshift, can explain these various redshift-dependent trends.

Notwithstanding this considerable progress, a major concern is that the above conclusions rest largely on deductions made with *photometric data*, particularly for the Lyman break population. Quite apart from the possibility of low-redshift interlopers lying within the photometric samples (a problem that increases for drop-out selected samples at redder wavelengths), the wanted physical measures of the star formation rate, dust content and stellar mass are all rendered uncertain by the absence of precise spectroscopic redshifts. While considerable effort has been invested in the spectroscopic study of $z \simeq 3$ LBGs (e.g. Shapley et al. 2003; Steidel et al. 2003; Quider et al. 2010), comparably little spectroscopy has been achieved for higher redshift samples. Steidel et al. (1999) obtained spectroscopic redshifts for nearly 50 bright ($I < 25$) $z \simeq 4$ LBGs. Most surveys of $z \simeq 5$–6 V and i' drops have generally involved relatively small samples, typically comprising fewer than 10 sources (e.g. Stanway et al. 2004, 2007; Ando et al. 2007; Dow-Hygelund et al. 2007). Recent deep *Hubble Space Telescope* (*HST*) Advanced Camera for Surveys (*ACS*) Grism observations of the Hubble Ultra Deep Field have allowed the spectra of faint $z \simeq 5$ LBGs to be characterized (Rhoads et al. 2009), albeit at very low spectral resolution, resulting in 39 redshift confirmations. The largest spectroscopic sample of $4 < z < 6$ LBGs thus far published is the VLT/FORS2 survey of the Chandra Deep Field South (Vanzella et al. 2002, 2005, 2006, 2008, 2009). This survey represents a major step forward, targeting 195 B-, V- and i'-drop galaxies and securing high redshifts for 99 of them. In addition, a recent campaign with the Visible MultiObject Spectrograph (VIMOS) spectrograph on the VLT has also targeted bright $z \gtrsim 3.5$ LBGs ($i'_{775} < 25$) in the Chandra Deep Field South, confirming redshifts for 20 bright sources at $3.5 < z < 5.5$ (Balestra et al. 2010).

We build on these strides in this paper, the first in a series presenting the results of a new Keck survey of $3 < z < 7$ LBGs selected photometrically in the Great Observatories Origins Deep Survey (GOODS) fields. The overall goal is to improve our understanding of the evolution of star-forming galaxies during the first 2 Gyr of cosmic history. Fully exploiting the 10 m Keck aperture, we have designed our survey to target intrinsically fainter sources than those reached in the VLT/FORS2 survey, thereby complementing that effort. Spectroscopy spanning a wide range of intrinsic luminosities is very important if we seek to understand earlier examples of the luminosity-dependent trends seen at $z \simeq 3$ (Reddy & Steidel 2009). As discussed below, it is equally important to target and study sub-luminous star-forming sources at early times, as these may be typical of those galaxies responsible for cosmic reionization (Bouwens et al. 2007; Ouchi et al. 2009; Bunker et al. 2010; Oesch et al. 2010; McLure et al. 2010).

Understanding evolution in the demographic trends of star-forming galaxies over $3 < z < 7$ is vital if we are to use galaxies as tracers of *cosmic reionization*, a cosmic event which is now a frontier of observational cosmology. Knowledge of when reionization occurred is crucial to our understanding of the nature of the earliest UV-emitting sources as well as the discrepancy between the observed number of dwarf galaxies and those expected from cosmological simulations (e.g. Salvadori & Ferrara 2009). Current observational constraints are limited. *Wilkinson Microwave Anisotropy Probe* (*WMAP*) measurements indicate that the Universe may have been partially ionized as early as $z \simeq 11$ (Dunkley et al. 2009; Larson et al. 2010), while observations of transmission in the spectra of quasars reveal that intergalactic hydrogen must be highly ionized below $z \lesssim 6$. While the discovery of an accelerated decline and increased variance in the mean transmitted flux from quasars initially led many to suggest that the intergalactic medium (IGM) is still partially neutral at $z \simeq 6.2$ (Fan et al. 2006), recent work has demonstrated that these results do not necessarily require a sudden change in the ionization state of the IGM (Becker, Rauch & Sargent 2007). Given the difficulty in locating quasars at $z > 7$, it seems unlikely that quasar spectroscopy will constrain the epoch when the bulk of the IGM was reionized in the near future.

Lyα emitting galaxies offer a valuable additional probe of the IGM (e.g. Rhoads & Malhotra 2001; Malhotra & Rhoads 2004; Kashikawa et al. 2006). In principle, the test is straightforward to apply. Young galaxies emit copious amounts of Lyα photons, which are resonantly scattered by neutral hydrogen. Hence, as we probe the regime when the IGM becomes significantly neutral, the fraction of star-forming galaxies showing strong Lyα emission should decrease (e.g. Haiman & Spaans 1999; Santos 2004; Furlanetto, Zaldarriaga & Hernquist 2006; McQuinn et al. 2007; Mesinger & Furlanetto 2008; Iliev et al. 2008; Dayal, Maselli & Ferrara 2010). Recent measurements of the LF of LAEs selected via narrowband imaging have revealed a tantalizing decline between $z = 5.7$ and $z = 7.0$ (e.g. Kashikawa et al. 2006; Iye et al. 2006; Ota et al. 2008), offering possible evidence that the ionization state of the IGM evolves over $6 < z < 7$.

Regardless of the validity of claims for an increasing fraction of neutral hydrogen over $6 < z < 7$, in practice the interpretation of the Lyα test is more complex. While the ionization state of the IGM affects the Lyα LF, so does evolution of a multitude of other properties intrinsic to the sampled population (e.g. Verhamme, Schaerer & Maselli 2006; Verhamme et al. 2008; Atek et al. 2008). Evolution in the dust content (Bouwens et al. 2009b), the column density, kinematics and geometrical distribution (generally described as the 'covering fraction') of neutral hydrogen (Shapley et al. 2003; Quider et al. 2009, 2010; Steidel et al. 2010) can each play a key role. Also important for the transmission of Lyα photons is the density of the IGM, which evolves continuously with redshift, and the

stellar initial mass function (IMF) of galaxies, for which few robust constraints exist at high redshift.

The existence of these complicating factors highlights the importance of understanding how the prevalence of Lyα-emitting galaxies varies just after reionization in addition to characterizing the decline that may occur during reionization itself. With this goal in mind, we seek to construct an independent measure of the redshift evolution of Lyα emitting galaxies over a large redshift baseline, complementary to past efforts (e.g. Ota et al. 2008). Here, we introduce the method of measuring the fraction of strong Lyα emitters (hereafter the 'Lyα fraction') within the LBG population. Applying the Lyα fraction test to a large sample of LBGs has many advantages. First, the LBG samples are already in place over $4 < z < 8$ owing to deep surveys with *HST* (e.g. McLure et al. 2010; Bunker et al. 2010; Bouwens et al. 2010b); hence the only time investment required is follow-up spectroscopy. This spectroscopy not only provides a sample of LAE with known spectroscopic redshifts, but also provides information on the kinematics of the interstellar medium (ISM; e.g. Shapley et al. 2003; Vanzella et al. 2009; Steidel et al. 2010) for individual bright sources (and for faint systems via composite spectra) and improves estimates of dust obscuration via UV colours, both of which are key factors governing the transmission of Lyα photons. By improving our understanding of how these properties change with time, we can begin to isolate the effect of reionization on the evolution in the Lyα fraction. Additionally, the Lyα fraction is insensitive to the declining number density of star-forming galaxies, in contrast to the Lyα LF test (which requires comparison to the UV LF to account for this degeneracy). Naturally, the Lyα fraction test has its own complications, but we show that these can be corrected for (see Sections 3.3 and 3.4), and we thus argue that this test will provide valuable constraints on reionization as new $7 < z < 10$ LBGs emerge in the next several years.

Our goal is therefore to obtain a robust measure of the luminosity and redshift dependence of the Lyα fraction when the IGM is highly ionized ($z \simeq 3$–6) and to compare it to the Lyα fraction at progressively earlier times. If the IGM ionization state evolves significantly at $z \gtrsim 6$ as possibly implied by the narrowband Lyα results, we would expect the measured fraction of LBGs with strong Lyα emission to be lower at $z \simeq 6$–8 than expected from extrapolating the trends seen over $3 < z < 6$. By placing the evolution of the Lyα fraction at $3 < z < 6$ in the context of the evolution of the well-characterized LBG parent population (e.g. variation of dust extinction with redshift and luminosity), we will calibrate the relative importance of factors other than reionization on the transmission of Lyα photons.

Our Lyα fraction test is ideally suited to our large spectroscopic sample of continuum-selected LBGs spanning the redshift range $3 \lesssim z \lesssim 7$. The current Keck sample (including a sample of archival i' drops to be presented in Bunker et al., in preparation) consists of 455B, V, i' and z drops (photometrically selected to lie at $3.5 < z < 7.0$) spanning a wide range in UV luminosity (to $M_{\rm UV} \simeq -18$). We combine this sample with a more luminous publicly available FORS2 data set of 195 sources satisfying photometric criteria similar to those adopted for the Keck surveys. Using this large spectroscopic data base, we address the primary goal of this first paper in our series – to compute the Lyα fraction as a function of luminosity and redshift. This will enable us to identify the principal factors governing its evolution over $3 \lesssim z \lesssim 6$, prior to extending the test to $6 \lesssim z \lesssim 8$, where we can probe changes in the IGM.

The plan of the paper is as follows. In Section 2, we describe the target selection and spectroscopic observations, and present the rest-frame UV properties of our current sample. In Section 3, we describe the construction of the Lyα catalogue, discuss the method used to measure Lyα equivalent widths and compute the completeness of Lyα detection as a function of luminosity and redshift. In Section 4, we discuss the luminosity dependence of Lyα emission in the context of earlier studies at $z \simeq 3$. We then turn to the redshift-dependence of Lyα emission and discuss the important implications of our findings. Finally, in Section 5, we examine the extant data on the rate of occurrence of Lyα emission for candidate sources thought to lie beyond $z \simeq 6$. We use this to test the practicality of using our test as a valuable probe of cosmic reionization. We summarize the conclusions of our study in Section 6.

Throughout the paper, we adopt a Λ-dominated, flat Universe with $\Omega_\Lambda = 0.7, \Omega_{\rm M} = 0.3$ and $H_0 = 70\,h_{70}\,{\rm km\,s^{-1}\,Mpc^{-1}}$. All magnitudes in this paper are quoted in the AB system (Oke & Gunn 1983).

2 OBSERVATIONS

We present the results of a new and ongoing Keck spectroscopic survey of photometrically selected B-, V- and i'-band 'dropouts' in the northern and southern GOODS fields (Giavalisco et al. 2004b). The GOODS fields were selected for this survey on account of the depth and precision of their unique multi-colour photometric data useful for selecting targets, as well as the availability of associated *Spitzer* and Chandra data which provided valuable stellar masses and active galactic nuclei (AGN)-related properties (Eyles et al. 2005; Yan et al. 2006; Eyles et al. 2007; Stark et al. 2007a, 2009; González et al. 2010; Labbé et al. 2010).

2.1 The Keck/DEIMOS survey in GOODS-N and GOODS-S

The majority of spectra discussed in this paper were obtained from an ongoing survey undertaken with the DEep Imaging Multi-Object Spectrograph (DEIMOS) at the Nasmyth focus of the 10-m Keck II telescope (Faber et al. 2003). DEIMOS comprises eight 2k × 4k CCDs spanning roughly half of the ACS GOODS field of view ($\simeq$16.7 × 5.0 arcmin^2) on the sky. Our first observations have primarily focused on targeting the B- and V-drop populations. Although future DEIMOS observations will expand coverage of higher redshift i'- and z-band dropouts, we include early data taken in this territory, some of which is described independently in Bunker et al. (2010, in preparation).

The recently studied target list is primarily selected from the B, V and i' dropout samples discussed in Stark et al. (2009). To this we will add earlier Keck data on i' drops discussed in Section 2.2 (Bunker et al. 2003; Stanway et al. 2004; Bunker et al. 2010, in preparation) as well as newly discovered z drops from the recent WFC3/IR Ultra Deep Field (UDF) campaign (see below). *Hubble* ACS imaging of the GOODS fields (Giavalisco et al. 2004b) provided deep optical images in F435W (B_{435}), F606W (V_{606}), F775W (i'_{775}) and F850LP (z_{850}). Optical magnitudes range from relatively bright systems ($z_{850} \simeq 23.5$) to the faintest dropouts observed in GOODS ($z_{850} \simeq 27.5$). Although the ACS photometry in Stark et al. (2009) was based upon the GOODS version r1.1 ACS multi-band source catalogues, for this analysis we have updated the photometry to the recently released GOODS version 2.0 catalogues. These new catalogues contain significantly deeper z_{850}-band imaging. With these catalogues, we compute optical colours using 0.5 arcsec diameter aperture photometry. After applying small aperture corrections to the colours which account for the fraction of flux which lies outside the photometric aperture area (see Stark et al. 2009 for details),

Table 1. Summary of observations with Keck/DEIMOS and VLT/FORS2. N_B, N_V, N_i, N_z denote the number of B, V, i' and z drops observed on each mask. To maximize S/N, many sources were observed on multiple DEIMOS masks; we account for such duplication when computing the total Keck sample size. The i' drops in the first two rows were originally published in Bunker et al. (2003) and Stanway et al. (2004), and the i' drops presented in rows 3 and 4 are from Bunker et al. (2010, in preparation). The VLT FORS2 sample is taken from observations presented in Vanzella et al. (2009). The combined total sample in the last row includes all unique dropouts in the Keck and VLT surveys.

Number	Field	Mask ID	Date	t_{exp} (ks)	N_B	N_V	N_i	N_Z	Grating
1	GOODS-S	GS031	2003 January 08–09	19.8	0	0	3	0	1200
2	GOODS-N	GN031	2003 April 02–06	37.8	0	0	5	0	1200
3	GOODS-S	GS041	2004 December 11	21.9	0	0	20	0	1200
4	GOODS-S	GS051	2005 October 31, November 01–02	8.4	0	0	17	0	1200
5	GOODS-S	GS071	2007 November 10–11	18.0	7	7	0	0	1200
6	GOODS-N	GN081	2008 April 03–05	21.6	85	9	0	0	600
7	GOODS-N	GN082	2008 April 03–05	21.6	95	12	0	0	600
8	GOODS-N	GN083	2008 April 03–05	20.4	86	14	0	0	600
9	GOODS-N	GN094	2009 March 24–26	18.0	45	63	0	0	600
10	GOODS-N	GN095	2009 March 24–26	25.2	43	36	0	0	600
11	GOODS-S	GS091	2009 October 19	19.2	0	0	19	17	830
Total unique Keck/DEIMOS sample					268	95	64	17	–
Total unique VLT/FORS2 sample					83	56	56	0	–
Combined unique sample					351	151	108	17	

we add the optical colours to the total z_{850}-band magnitude (determined from the SExtractor MAG_AUTO parameter; see Bertin & Arnouts 1996) to derive total magnitudes in the B_{435}, V_{606} and i'_{775} ACS bands. We ensure that the continuum flux estimates for our DEIMOS sample correspond to entire galaxies and not individual clumpy components that would not be resolved in our seeing-limited spectroscopic observations. The 5σ limiting magnitudes vary across the different frames, but are typically 28.0 in B_{435}, 28.2 in V_{606}, 27.9 in i'_{775} and 27.8 in z_{850} when measured in 0.5 arcsec diameter apertures. At the median redshifts expected for these populations ($z = 3.8$ for B drops, $z = 5.0$ for V drops and $z = 5.9$ for i' drops; e.g. Bouwens et al. 2007), these limits correspond to absolute magnitude limits of $M_{UV} \simeq -18.2$, -18.8 and -19.1 for B, V and i' drops.

A summary of the various observing campaigns is given in Table 1. Apart from the i'-drop exploratory survey discussed by Bunker et al. (2010, in preparation), in our campaigns during 2004–2007 targets were selected to fill empty regions on slitmasks designed for other purposes, e.g. studying the kinematics of disk galaxies at $z \simeq 1$ (MacArthur et al. 2008). For these observing runs, we used the Gold 1200 line mm^{-1} grating which provided coverage between 5570 and 8210 Å (allowing Lyα to be detected in the redshift range $z = 3.6$ to 5.8), with a spectral pixel size of 0.3 Å pixel^{-1}. We used a slitwidth of 1 arcsec, with slit lengths varying between 6 and 12 arcsec^2 depending on the presence of nearby objects on the slitmask. The spectral resolution measured from skylines was 1.4 Å.

The main survey began in earnest in 2008, when we started a dedicated programme geared at obtaining spectra of $z > 3$ dropouts. Most spectra were obtained from five slitmasks observed in 2008 April and 2009 March (Table 1). These slitmasks utilized the 600 line mm^{-1} grating on DEIMOS, providing spectroscopic coverage between 4850 and 10150 Å (allowing Lyα to be detected between $z \simeq 3.0$ and 7.3) with a spectral pixel scale of 0.7 Å pixel^{-1}. We again used a slitwidth of 1 arcsec, with slit lengths varying between 6 and 12 arcsec. These spectra provided a resolution (measured from skylines) of $\simeq$3.5 Å. This setup allowed us to efficiently follow-up B- and V-band dropouts simultaneously. Each individual mask was observed for $\simeq$5–7 h and contained $\simeq$80–110 dropouts. Seeing was typically 0.8 arcsec, ranging between 0.5 and 1.0 arcsec.

We observed a final slitmask towards GOODS-S on 2009 October 19–20. For this run, we prioritized i' drops and newly discovered z drops (Oesch et al. 2010; McLure et al. 2010; Bunker et al. 2010; Wilkins et al. 2010a) and therefore opted for the higher resolution 830 line mm^{-1} grating blazed at 8640 Å with order blocking filter OG550. We adopted the same slitwidths and typical lengths as in our previous campaigns. With this set-up, the spectra generally provide coverage between 6800 and 10 100 Å (allowing Lyα to in principle be detected between $z = 4.5$ and 7.3), with each spectral pixel spanning 0.46 Å. Skylines are measured to have a full width at half-maximum (FWHM) of $\simeq$2.4 Å, a significant improvement upon the resolution obtained with the 600 line grating. However, poor seeing (average of 1.3 arcsec) and fog made redshift confirmation particularly difficult.

All data were reduced using the spec2d IDL pipeline developed for the DEEP2 Survey (Davis et al. 2003).[1] The final reduction provides two-dimensional (2D) spectra and variance arrays, along with a one-dimensional (1D) extraction at the expected position of the dropout. Wavelength calibration was typically obtained from Ne+Xe+Cd+HG+Zn reference arc lamps. In general, the final wavelength solution is accurate to within $\simeq$0.1 Å. Examples of reduced 1D spectra are presented in Fig. 1.

We flux calibrated the spectra using spectroscopic standard stars observed in the 2009 March 24–26 observing run. We tested the flux calibration derived from these standards using spectra of alignment stars included on the slitmask (observed in 2×2 arcsec^2 boxes). We compute optical broad-band magnitudes for the alignment stars from the flux-calibrated spectra using the appropriate filter transmission functions. The magnitudes measured from the spectra match those from the ACS images to within a factor of $\simeq 2$. We bootstrapped a flux calibration on spectra from observing runs for which spectroscopic flux standards were not taken (2008 April 03–05) using the measured flux in alignment stars that are in common between the 2008 and 2009 observing runs. We note that atmospheric dispersion does not significantly alter the measured flux from our dropout samples. Where possible, we

[1] The spec2d pipeline can be downloaded at http://juno.as.arizona.edu/cooper/deep/spec2d/

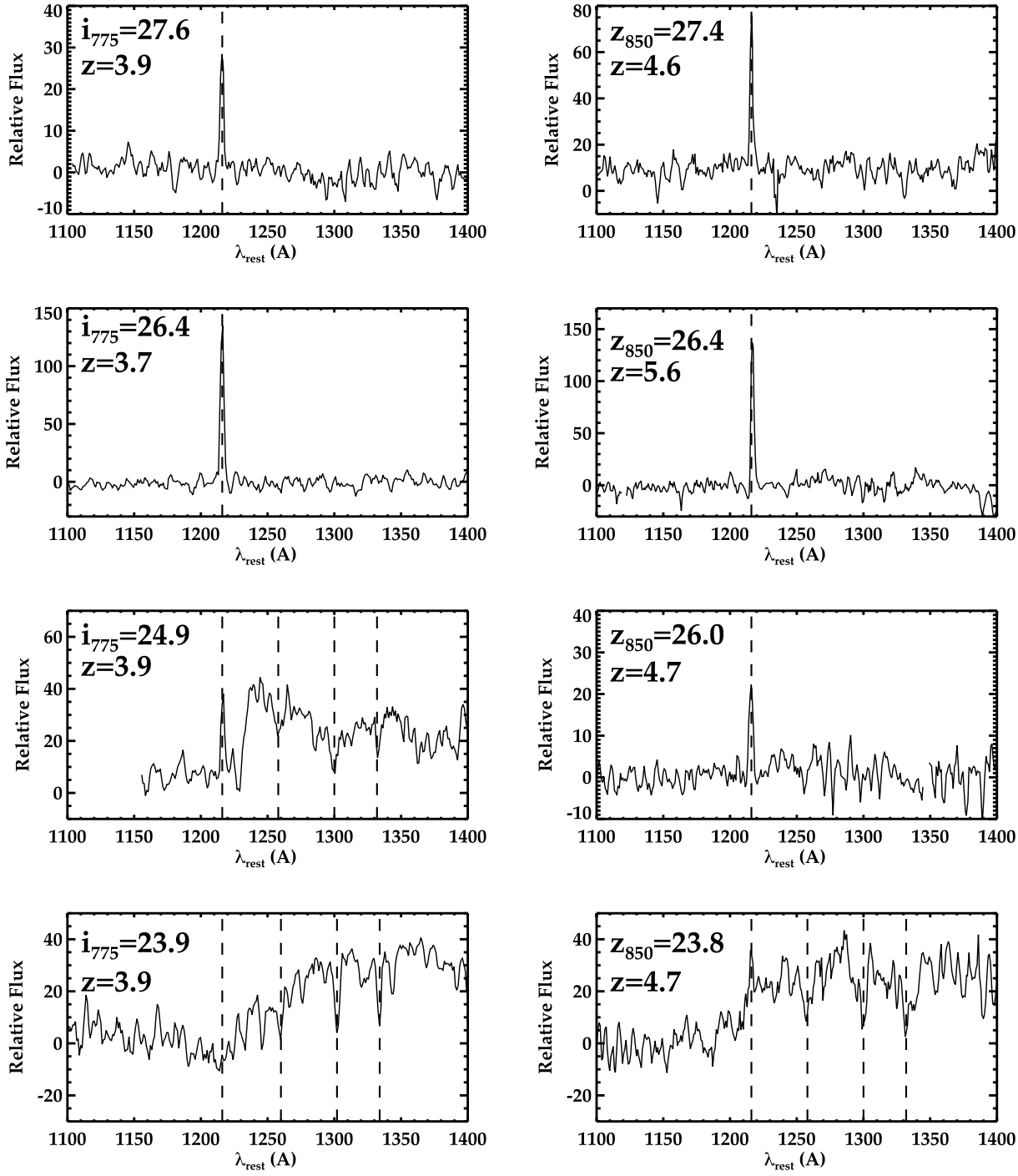

Figure 1. Montage of DEIMOS 1D spectra from our survey arranged according to redshift and luminosity. *B* drops are shown in the left-hand column, and *V* drops appear in the right-hand column. Each panel contains a label indicating the apparent magnitude of the continuum and redshift. Spectra are smoothed to a spectral pixel size of ≃3 Å. Where present, dashed vertical lines denote Lyα, Si II 1260, O I+Si II 1303 and C II 1334 lines.

have aligned the mask (and slit) position angles along the mean parallactic angle. In the few masks where this was not possible, given our typical observational set-up, we estimate a flux differential of no more than ≃5 per cent (Filippenko 1982) from the blue end of our *B*-drop sample to the red end of the *V*-drop sample.

Using the flux calibrations, we compute our typical 1σ flux sensitivity across the DEIMOS spectra for the 600 line grating. These measurements predict that we should detect continuum at the 1σ level for sources with $V_{606} \simeq 25.5$ or 1.9×10^{-19} erg cm^{-2} s^{-1} A^{-1} (per spectral resolution element in 1D spectra which have been extracted over ≃1 arcsec) across much of the wavelength regime covered by the 600 line spectra. This prediction is consistent with expectations based on the optical magnitudes of sources that show continuum traces in the spectra. The average 10σ limiting line flux is 1–1.5 $\times$ 10^{-17} erg cm^{-2} s^{-1} between 6500 and 9300 Å, although sky lines become much more common towards the red side of the spectra. In a later section, we present more detailed simulations

that reveal the completeness for emission lines of a given flux and redshift.

For the most recent run (2009 October), the limiting sensitivity was significantly worse than in previous runs due to the seeing and fog. Based on the signal obtained from the bright alignment stars on the mask (each of which has known broad-band magnitudes) and the signal from our spectroscopic standard stars, we estimate that our continuum 1σ sensitivity (computed per resolution element with a spatial extraction width of $\simeq$1.5 arcsec) was $i' \simeq 24.25$ or $\simeq 3.5$–4.0×10^{-19} erg cm^{-2} s^{-1} Å^{-1} in between sky lines. Assuming typical linewidths, this limit translates into a 10σ line flux limit of 2.5–4.0 $\times$ 10^{-17} erg cm^{-2} s^{-1} for Lyα. As most of the sources targeted in this run were faint ($z_{850} > 26$ for the i' drops), this means that we are only sensitive to very strong emission lines (the 10σ rest-frame equivalent width limit is $\simeq$75–100 Å for sources with $z_{850} \simeq 26.5$). For fainter sources (e.g. the majority of WFC3 z drops in the UDF), the equivalent width limits are too large to enable the detection of Lyα.

To summarize the current status of our DEIMOS observations, we have obtained 549 spectra of B, V, i' and z drops. To boost the signal-to-noise ratio (S/N) of our spectra, many dropouts were observed on multiple masks; hence, each spectra does not correspond to a unique source. Accounting for this, we observed a total of 268 B drops, 95 V drops, 19 i' drops and 17 z drops. We combine this sample with archival Keck and VLT spectra in the following two subsections, and in Section 2.4, we present the absolute magnitude distribution of the combined VLT and Keck spectroscopic samples.

2.2 Archival Keck spectroscopy in GOODS-N/S

Additional i' drops were observed with Keck/DEIMOS between 2003 and 2005 (Table 1). Early observations were presented by Bunker et al. (2003) and Stanway et al. (2004), and an updated discussion, including additional DEIMOS observations from 2003–2005, is given by Bunker et al. (2010). These sources were observed with the 1200 line mm^{-1} (described above) with seeing of 0.7 to 1.0 arcsec. Slitwidths were 1.0 arcsec, identical to our more recent DEIMOS observations described above.

In total, 45 i' drops were observed in the two GOODS fields on four separate slitmasks. Of the 45 sources observed, 12 were included in the Vanzella et al. (2009) VLT/FORS observations discussed below. Integration times ranged between 2.3 and 10.5 h. The z_{850}-band magnitudes of the sources ranged between 24.7 and 28.3. Given the considerable range of exposure times, we take care to estimate the equivalent width completeness for sources of different magnitudes on the various masks that were observed.

2.3 Archival VLT/FORS spectroscopy in GOODS-S

Two programmes aimed at following up high-redshift dropouts in GOODS-S have been conducted with the VLT. The first of these used the FORS2 multi-object spectrograph (Vanzella et al. 2005, 2006, 2008, 2009), and the second used the VIMOS multi-object spectrograph (Balestra et al. 2010). Both teams have released their data sets to the public. In this paper, we focus on the FORS2 survey, as its survey characteristics (resolution, spectral coverage) are closest to the DEIMOS survey. We discuss the basic FORS2 survey details below.

Between 2002 September and 2006 October, the VLT FORS2 multi-object spectrograph was used to observe sources identified in the GOODS imaging of Chandra Deep Field South (CDF-S). In total, 38 FORS2 masks were obtained using the 300I grism

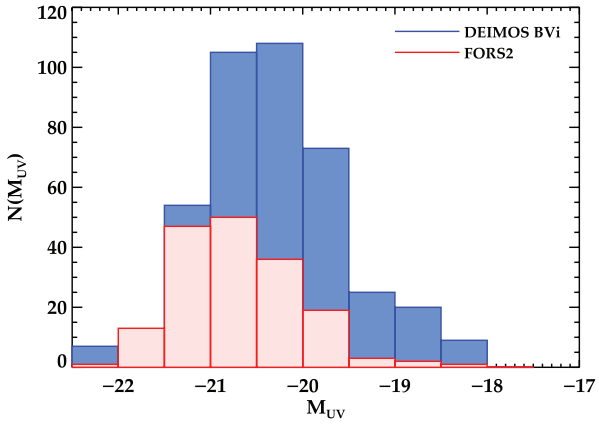

Figure 2. Absolute magnitude distribution of FORS and DEIMOS spectroscopic samples. The new DEIMOS B, V and i' drops are shown in shaded blue, and below the FORS2 observations (Vanzella et al. 2009) are shown in light red. The DEIMOS data sets comprise the majority of the spectra considered in our analysis.

without an order-separating filter. Slitwidths were 1.0 arcsec in all observations. Each mask was observed for roughly 4–6 h. In general, the spectra provide coverage between 6000 and 10 000 Å, with a spectral resolving power of $R = 660$ which provides resolution of $\simeq$13 Å at 8600 Å.

The FORS2 data base provides redshift classifications and quality grades (ranging from A to C) for the entire spectroscopic sample. The colour criteria used to select the dropouts in the FORS2 sample are discussed in Giavalisco et al. (2004a); however, for the B drops, a slight variation in the colour selection was adopted (for details see Vanzella et al. 2009).

In general, these criteria are very similar to those we have adopted for our DEIMOS survey. Using the coordinates provided in the public FORS2 data base, we query the version 2.0 ACS catalogues for GOODS-S and measure optical magnitudes in an identical fashion as described in Section 2.1. Adopting the selection criteria used for the DEIMOS sample (see Stark et al. 2009), we find 83 B drops, 56 V drops and 56 i' drops that were observed with FORS2. Redshifts were obtained for 48 B drops (46 with $z > 3$), 37 V drops (32 with $z > 4$) and 26 i' drops (21 with $z > 5$).

The magnitude distribution of the FORS2 sample is generally weighted towards brighter sources, with few B and V drops with magnitudes fainter than $z_{850} \simeq 26$. Given the inherent faintness of i'-drop samples, the magnitude distribution is significantly fainter than for the lower redshift dropout samples, with $z_{850} \simeq 25$–27. In Fig. 2, we plot a comparison of the absolute magnitude distribution of the FORS2 and DEIMOS dropout samples. The current DEIMOS sample contributes 76 per cent of the B drops and 63 per cent of the V drops and crucially extends the spectroscopic coverage to lower luminosities.

2.4 Final spectroscopic sample

When combined, the FORS2 and DEIMOS surveys contain a total of 627 spectra of unique high-redshift dropouts (351 B drops, 151 V drops, 108 i' drops and 17 z drops). In Fig. 3, we present colour–colour diagrams of the entire B- and V-drop spectroscopic sample, indicating the selection criteria. The i' drops were selected using the standard single $i' - z > 1.3$ colour criterion (see Fig. 4). Comparing the distribution of selected targets on these figures with the larger sample of sources in the Stark et al. (2009) photometric catalogue,

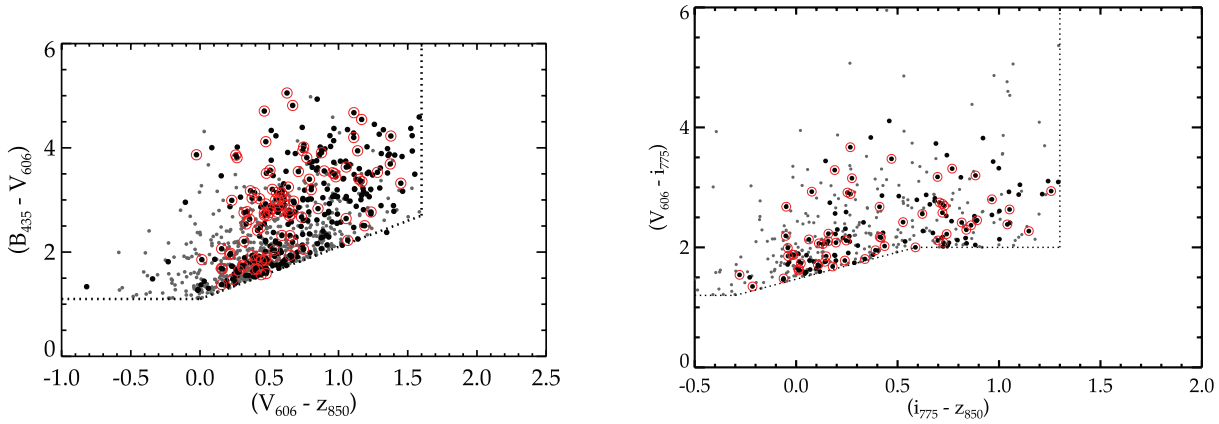

Figure 3. Colour–colour diagrams for the *B* drops (left) and *V* drops (right). The small grey filled circles show the distribution of colours for the parent population of LBGs from Stark et al. (2009), while the large black filled circles denote those objects in the combined Keck and VLT spectroscopic survey discussed in this paper. Open red circles denote those objects with Lyα in emission. The dotted lines show the Lyman break selection criteria adopted in this paper.

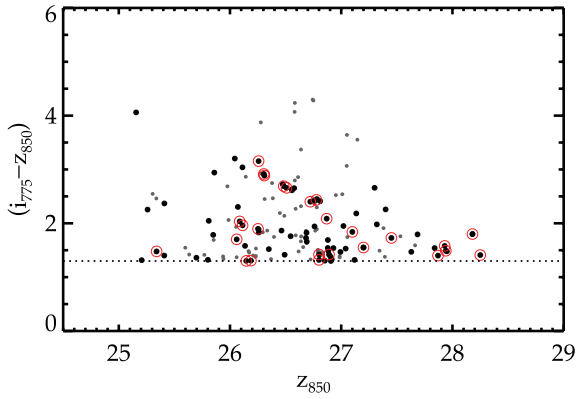

Figure 4. $i' - z$ colour versus magnitude for i' drops with spectroscopic observations with the dashed line showing the selection cut. Points surrounded by a red open circle indicates sources with Lyα seen in emission, and the small grey circles indicate the colours and magnitudes of i' drops from the parent LBG samples (Stark et al. 2009).

we demonstrate that the colours of our targets with spectroscopic coverage span nearly the full range of the parent LBG population.

Fig. 5 also shows the apparent magnitude distributions of the various dropout samples. While previous surveys have focused on sources with apparent magnitudes brighter than $m \simeq 26$, a major achievement of our survey is that we have been able to push significantly below this limit with DEIMOS. Our primary motivation for doing so is that the characteristic UV luminosity shifts to lower values at higher redshifts (e.g. Bouwens et al. 2007), so to compare source properties over $3 \lesssim z \lesssim 7$ in a meaningful manner, probing deep becomes a necessity. To demonstrate our survey has achieved this over $3 < z < 6$, in Fig. 6, we compare the absolute magnitude distribution of our various dropout samples. Current estimates of the characteristic absolute magnitude at $z \simeq 7$ are $M_{\rm UV} \simeq -19.9 \pm 0.09$ (Bouwens et al. 2009a; Ouchi et al. 2009; Oesch et al. 2010). As objects more luminous than this are exceedingly rare at $z \gtrsim 6$–7, if we are to make consistent Lyα fraction comparisons, we must probe to at least this depth over $4 < z < 6$.

Redshifts were determined via the visual examination of the spectra (see Fig. 7 for a redshift distribution). For UV faint sources, the continuum is too faint for identification of the Lyman break or absorption lines, so we can only measure spectroscopic redshifts for those sources with Lyα in emission. For UV bright sources, redshift identification is performed via a combination of the Lyman break, interstellar absorption lines and/or Lyα emission. We classify all redshifts according to their quality, ranging from A (definite), B (secure), C (possible/likely). We estimate that those objects with quality flags A, B and C are very roughly $\simeq$100, 95 and 70 per cent likely to lie at the classified redshift. Nearly all LAEs fall into the first two categories owing to the combination of line profile, lack of other emission lines and strong continuum break (in spectra and/or imaging), but some of the absorption line detections are much more tenuous owing to sky line residuals and noise. As the results of this paper are independent of the absorption line sample, we delay further discussion of the absorption line catalogue until a subsequent paper (Stark et al., in preparation), while details of the Lyα selection are described in the following section. However, we note that, in total, the FORS2+DEIMOS sample contains 179 redshifts over $3 \lesssim z \lesssim 4.5$, 87 redshifts over $4.5 \lesssim z \lesssim 5.5$ and 44 redshifts over $5.5 \lesssim z \lesssim 6.5$.

3 EMISSION LINE MEASUREMENTS

3.1 Constructing the Lyα catalogue

Emission lines were initially identified visually in the 2D DEIMOS spectra and later in the 1D extractions at the position of the dropouts. We took care to distinguish Lyα from other emission features which correspond to lower-redshift galaxies. In particular, [O II] emission (which is resolved by DEIMOS) is identified in five *B*-band dropouts. Lyα emission is detected in 152 of the DEIMOS dropouts.

For the VLT/FORS data set, the redshifts were determined in Vanzella et al. (2009). As discussed in Section 2.3, to ensure a uniform selection across the Keck and VLT samples, we performed our own photometric selection. With the resulting subset of 193 galaxies, we identified those objects showing Lyα in emission in their 1D spectra.

We defined Lyα redshifts ($z_{\rm Ly\alpha}$) for each object as the wavelength at which the Lyα line is at its peak flux value. As Lyα is generally redshifted by at least $\simeq$300 km s^{-1} from the frame of rest of the galaxy (e.g. Shapley et al. 2003; Vanzella et al. 2009), we note that this redshift is not necessarily equivalent to the systemic redshift of the galaxy. Across both surveys, we identified Lyα emission in 108 *B* drops, 63 *V* drops and 28 i' drops. The relative colour distribution

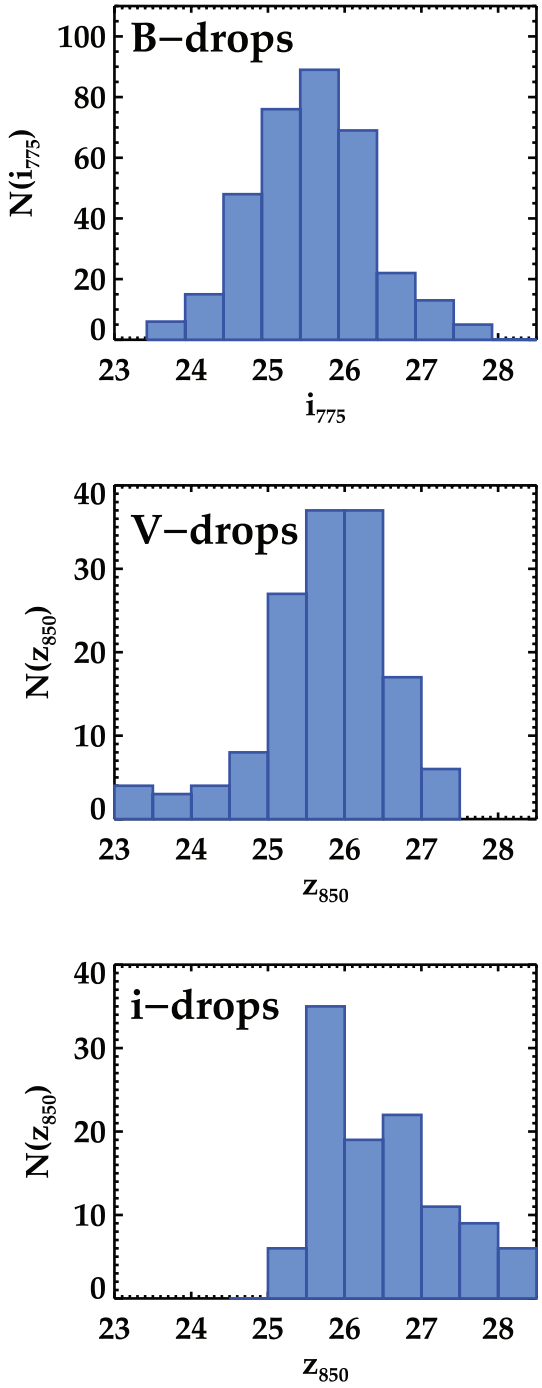

Figure 5. Distribution of apparent magnitudes of *B* drops (top), *V* drops (middle) and *i*′ drops (bottom) in combined Keck and VLT spectroscopic survey.

of these sources in relation to the larger spectroscopically targeted sample is shown in Figs 3 and 4.

In addition to the *B*, *V* and *i*′ drops, we present tentative spectroscopic confirmation for one of the *z* drops that was studied in poor conditions in the 2009 October DEIMOS run (Table 1). The only *z* drop to show a clear emission feature at the expected object location was source 3 in Wilkins et al. (2010a). This object, identified in the GOODS ERS WFC3 imaging of CDF-S (PI: O'Connell), is reasonably faint ($J_{125} \simeq 27.3$) but is brighter than most of the $z \gtrsim 6$ sources detected in the UDF (e.g. Oesch et al. 2010; Bunker

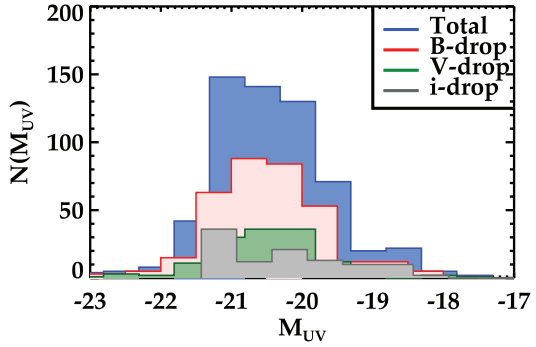

Figure 6. Distribution of absolute magnitudes of sources in the combined DEIMOS and FORS2 spectroscopic survey (shaded blue). The shaded light red, green and grey denote the magnitude distribution of the *B*-, *V*- and *i*′-drop samples.

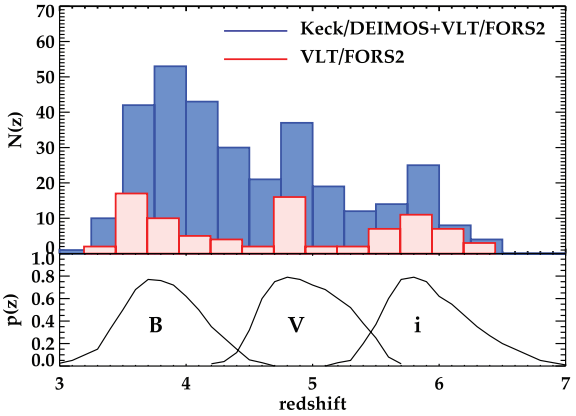

Figure 7. Redshift distribution of *B*, *V* and *i*′ drops with spectroscopic confirmation in GOODS-N and GOODS-S (dark blue). This sample includes absorption line systems in addition to the LAEs discussed in this paper. The total sample contains 179 galaxies with redshifts in the range $3 \lesssim z \lesssim 4.5$, 87 galaxies with redshifts over $4.5 \lesssim z \lesssim 5.5$, and 44 galaxies with redshifts over $5.5 \lesssim z \lesssim 6.5$. For reference, we display the redshift distribution of the VLT/FORS2 survey (Vanzella et al. 2009) in light red. In the bottom panel, we display the expected redshift distribution functions derived by Bouwens et al. (2007) from the observed optical photometric colours of the three dropout samples.

et al. 2010; McLure et al. 2010). The DEIMOS spectrum illustrates a significant 7σ emission line in between sky lines and centred at 9044 Å (Fig. 8). The S/N and nearby sky line do not enable a robust measure of the asymmetry of the line. The broad-band spectral energy distribution (SED) is well fitted by a source $z \simeq 6.44$ with strong Lyα contaminating the medium-band Y_{098} filter (Fig. 9). If this emission feature is Lyα, it would lie at $z = 6.44$, consistent with the photometric redshift predictions. Our flux calibration suggests a flux of 1.5×10^{-17} erg cm^{-2} s^{-1} and hence an equivalent width (rest frame) of 83 Å. We will confirm the redshift of this source in future campaigns of CDF-S.

3.2 Computation of Lyα properties

Next we compute the flux ($F_{\mathrm{Ly}\alpha}$) and equivalent width ($\mathrm{W}_{\mathrm{Ly}\alpha}$) for each LAE in our spectroscopic sample. Previous attempts to constrain evolution in the prevalence of LAE have focused on measuring evolution in the LF of LAE (selected via narrowband filters). For our Lyα fraction test described in Section 1, we are interested in determining the percentage of LBGs of a given luminosity with Lyα emission much stronger (e.g. >50 times in the rest frame) than the

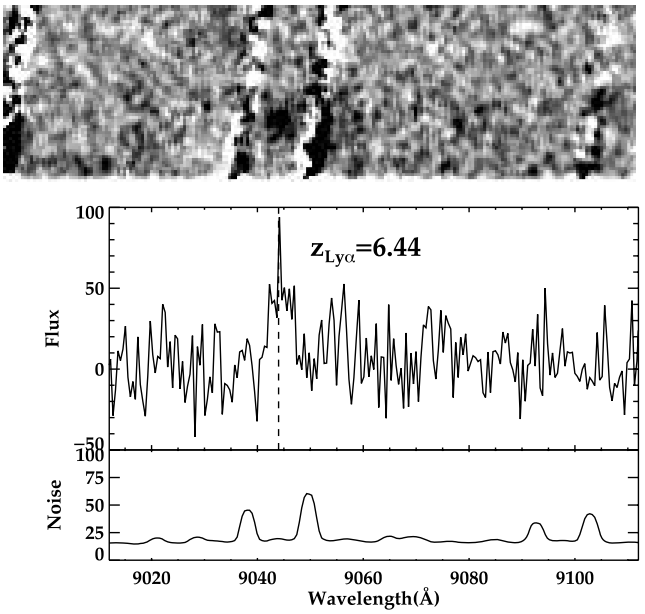

Figure 8. Spectra of a $J_{125} \simeq 27.3$ z drop showing tentative Lyα emission at 9044 Å. Top panel: the 2D spectrum shows a significant emission feature detected at the 7σ level (black corresponds to positive flux in the image) in between two sky lines and centred exactly at the position of z drop '3' in Wilkins et al. (2010a). Bottom panel: the 1D spectrum of the galaxy and associated noise. The spectrum and noise are not smoothed to avoid blending with skylines at 9038 and 9048 Å. The emission line between these features lies in a region of low noise, spanning $\simeq$ 10 Å in width.

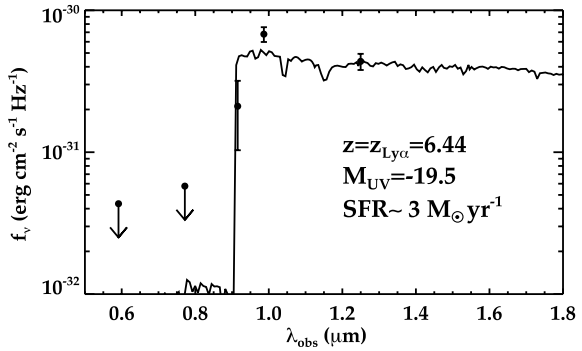

Figure 9. Spectral energy distribution of z drop '3' from Wilkins et al. (2010a). The data points show detections and upper limits from ACS and WFC3 imaging of CDF-S. Overplotted is a Bruzual–Charlot population synthesis model with a redshift fixed at $z = 6.44$, the spectroscopic redshift inferred from the emission line detected in Fig. 8. The broad-band imaging data show a prominent break where the Lyman break is predicted and a significant excess of flux in the medium-band Y_{098} filter (relative to the J_{125} band), as expected in the presence of strong Lyα emission.

continuum flux. This test thus relies on accurate measurements of the Lyα equivalent widths ($W_{Ly\alpha}$).

In principle, $W_{Ly\alpha}$ provides a more robust constraint than $F_{Ly\alpha}$ as it does not rely on an absolute flux calibration. However, since the majority of spectra in our sample have broad-band continuum magnitudes fainter than the 1σ continuum flux limit of our survey ($m \simeq$ 25–26, Section 2.1), we can only place an upper limit on the continuum flux measured in this subset of our spectra, thus producing a lower limit to the observed $W_{Ly\alpha}$. We can obtain a better estimate of the equivalent width by adopting the continuum flux measured from broad-band imaging, taking care to avoid filters that are contaminated by Lyα. We detail the specific procedure used to measure $W_{Ly\alpha}$ below.

For each spectrum, we compute the line flux, $F_{Ly\alpha}$, by summing emission in excess of the continuum between 1213 and 1221 Å, taking care to avoid contribution from nearby sky lines or artefacts and ensuring that the spatial extraction along the slit covers the entire spatial width of the line emission. The spatial extraction width was typically $\simeq$1 arcsec in length.

The measurement of the continuum flux depends on whether or not continuum is detected. For those objects with continuum detections, we compute the average continuum level redwards of Lyα, c_{red}, by averaging the flux in regions between OH sky lines between 1225 and 1255 Å in the rest frame of the galaxy. As discussed in Kornei et al. (2010), this should minimize the contribution from nearby absorption features. The observed-frame $W_{Ly\alpha}$ is then computed by taking the ratio of $F_{Ly\alpha}$ and c_{red}, where by definition the continuum has been subtracted from the line flux. We compute the random error in the equivalent widths from the measured uncertainty in $F_{Ly\alpha}$ and c_{red}.

For those objects without continuum detections, we compute equivalent widths using the continuum level just redwards of Lyα with the broad-band photometry discussed in the previous section and taking care not to include the contribution of Lyα to the continuum. For the B- and V drops, we use the total i'_{775} and z_{850}-band fluxes, respectively. These measurements provide the luminosity at rest frame $\simeq$1500 Å, rather than just redwards of Lyα. The vast majority of sources are very blue (and hence nearly flat in f_ν), requiring no correction between the flux at 1500 Å and that at 1240 Å (the central value in the wavelength region summed for continuum measurements above). For those few sources with very red UV slopes (measured from the broad-band SEDs presented in Stark et al. 2009), we apply a small adjustment to correct for the change in flux between 1500 and 1240 Å. Before computing $W_{Ly\alpha}$, we subtract the continuum estimate from the measured line flux, although since these sources are so faint, this always ends up being a nearly negligible change to the derived equivalent width. We again compute σ_W from the measured uncertainty in the line and continuum flux. The combination of different photometric and spectroscopic apertures could in principle bias the equivalent width measures, but by computing the total continuum flux (as described in Section 2.1) and our best estimate of the total line flux (as described above), we seek to minimize these uncertainties. As we will demonstrate below and in Fig. 10, the general agreement between the equivalent widths of bright galaxies measured using directly from their spectra and those measured using the combined spectral and imaging data suggests that this approach is fairly successful.

For galaxies with redshifts above $z \simeq 5.7$, the z_{850}-band filter is contaminated by both Lyα emission, if emission is present, as well as Lyα forest absorption shortwards of rest 1216 Å. Accurate continuum determinations must account for this. If sources contain Y- or J-band detections via WFC3 or ISAAC, then we use these measures for the UV continuum. However, at the moment, the majority of UV-faint i' drops are not detected with significance in the near-IR, so we must use z_{850} detections for these sources. For galaxies with no detected Lyα emission, we must only correct for the Lyα forest absorption, which we do assuming the redshift is identical to its value inferred from the Bayesian Photometric Redshift (bpz) code and that its SED is flat in f_ν. Corrections range from $\simeq$0.2 mag at $z = 6$ to 0.7 mag at $z \simeq 6.4$. But for $z > 5.7$ objects with strong Lyα emission, we also subtract off the line contribution when computing the continuum flux. Typical line contributions are $\simeq$0.1–0.3 mag.

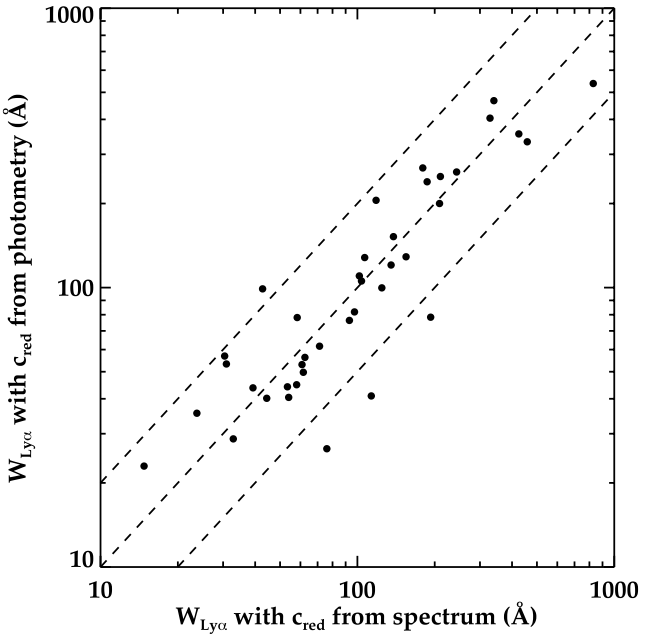

Figure 10. Reliability of $W_{Ly\alpha}$ measurements. The x-axis shows equivalent widths (observed-frame) determined directly from spectra for sources bright enough for a continuum measurement. The y-axis shows the equivalent widths measured for the same sources using the continuum flux from the broad-band photometry. The dashed lines demarcate values 0.5× and 2× the $W_{Ly\alpha}$ measured directly from the spectrum. The median fractional error from using equivalent widths derived using the continuum flux from broad-band imaging is ≃20 per cent.

To test the reliability of the above method, we examine the subset of galaxies with bright UV continua, comparing the continuum flux determined from broad-band imaging to that extracted from the spectra. We find that the median fractional error using the estimate from broad-band imaging is ≃20 per cent (Fig. 10). We compute the uncertainty in the equivalent width measurements, σ_W, by adding this error in quadrature to the random error on each equivalent width measurement.

3.3 Completeness of Lyα detection

In order to properly assess the fraction of LAE in our sample as a function of UV luminosity and redshift, we must consider how completeness varies with apparent magnitude and wavelength of the Lyα emission line. We estimate the typical completeness by adding fake Lyα emission to random positions across the DEIMOS and FORS2 spectra. In each case, we measure the line properties ($W_{Ly\alpha}$, $F_{Ly\alpha}$, S/N) of the fake emission feature. Fake emission lines were generated by one of the authors (KC) and then searched through by another (DPS) to ensure a fair test as close to the actual process of identifying observed emission lines as possible. We ran enough trials (using a large number of spectra from each mask) to obtain reliable estimates of the completeness of the Lyα recovery.

Our goal is to identify a lower flux threshold above which Lyα is highly complete for most objects in our sample in order to minimize the necessary completeness corrections. We illustrate the results of the completeness simulations for the 600 line mm^{-1} grating on DEIMOS in Fig. 11. The masks on this grating included B and V drops which span the redshift range $3.5 \lesssim z \lesssim 5.5$. The simulations reveal that sources with $m_{AB} \simeq 27.0$ and with rest-frame Lyα equivalent widths ($W_{Ly\alpha,0}$) in excess of 50 Å are generally recovered over nearly the entire redshift range probed by our dropouts (see Fig. 11). The high completeness for very strong LAE amongst bright sources ($m \lesssim 26$) arises as these bright emission features correspond to fluxes that are in excess of 10–20σ and are recovered even when they lie on top of sky lines. The $W_{Ly\alpha,0} > 50$ Å emission line completeness begins to decline for very faint sources ($i' \simeq 27.5$) at the high-z tail of the V-drop redshift distribution. For the FORS2 data, the spectra show similarly high completeness for B and V drops with $W_{Ly\alpha,0} > 50$ Å. These simulations suggest that the measured Lyα fraction of sources in the redshift range $3.5 \lesssim z \lesssim 5.5$ should not suffer from significant incompleteness for B and V drops more luminous than $M_{UV} \simeq -19$.

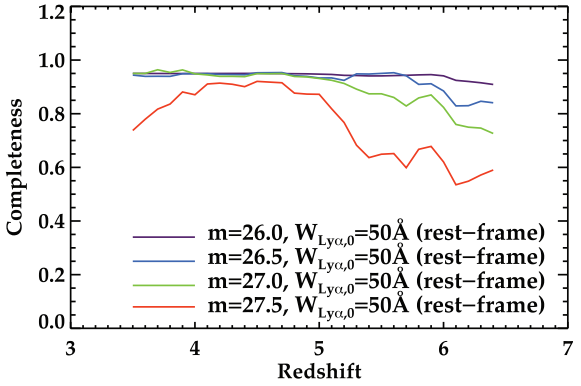

Figure 11. Emission line recovery completeness. The completeness is determined via simulations placing fake lines in spectra and testing the rate at which sources about the equivalent width threshold are recovered. From top to bottom, the figure shows completeness versus redshift for $W_{Ly\alpha,0}$ sources with continuum magnitudes (longwards of the Lyman break) of 26.0, 26.5, 27.0 and 27.5.

For the i' drops, the completeness in the deep DEIMOS and FORS2 spectra remains high for strong (e.g. $W_{Ly\alpha,0} > 50$ Å) Lyα lines. However, it is clear from Fig. 11 that incompleteness is not negligible, particularly for faint ($z_{850} > 27.0$) sources at $z \gtrsim 5.8$ which are less than 80 per cent complete. We thus adopt this as our i'-drop magnitude threshold for inclusion into the Lyα fraction test, limiting us to sources more luminous than $M_{UV} \simeq -19.7$. We also do not include the 17 i' drops on the mask GS051 (see Table 1) from Bunker et al. (2010, in preparation) owing to its reduced integration time of 2.3 h.

3.4 Contamination in spectroscopic samples

Although foreground emission line sources (e.g. [O II] emitters) can be readily distinguished from those revealing Lyα (Section 3.1), our Lyα fraction test requires that we have a reliable sample of LBGs for which no emission line is seen.

While the Lyman break selection criteria are chosen to minimize the inclusion of low-redshift and stellar contaminants, it is clear that interlopers still populate dropout samples. For our purposes, it is important that we consider the luminosity and redshift dependence of contaminants, as these could create artificial trends in our derived Lyα fractions. We expect low-z contamination to increase towards the fainter end of our sample. This is primarily due to photometric scatter; since faint sources are detected with lower S/N and have less dynamic range available to constrain the break, it is more likely that a faint low-z source will be scattered into the LBG selection window. However, if the typical contamination is fairly low in all luminosity bins (e.g. ≲10 per cent), then this would only require a minor correction to the luminosity dependence of the Lyα fraction.

To investigate this in more detail, we compute photometric redshift probability distributions for the spectroscopic sample using the observed photometric catalogues compiled in Stark et al. (2009), updated to include v2 GOODS ACS photometry, and the BPZ software (Benitez 2000). Details of the photometric redshift methodology are discussed in Stark et al. (2009). Using the probability distributions derived from BPZ, we compute the probability that each object lies outside the redshift range constrained by our spectroscopic observations (typically $z \lesssim 3.4$). We then place those galaxies without spectroscopic redshifts in bins of UV luminosity and compute the total contamination fraction as a function of UV luminosity. As expected, the results show that the contamination fraction increases toward lower luminosities. We find negligible contamination for bright sources ($-22 \lesssim M_{\rm UV} \lesssim -20$) with SEDs constrained by high S/N photometry. The low contamination values we find are consistent with simulations conducted by Bouwens et al. (2007) which indicate a contamination factor of an order of $\simeq$2–3 per cent. In the two faintest absolute magnitude bins considered ($M_{\rm UV} = -19$ and -18), the predicted contamination increases to $\simeq$10 per cent. This suggests that, owing to low-z contamination, the true Lyα fractions in the two faintest bins should be 1.11 times greater than derived. We consider the effects of this in our discussion of the Lyα fraction in Section 4.1.

We now examine whether contamination should vary strongly with redshift. As above, we measure the contamination fraction (of objects that are not LAE) implied for B-, V- and i'-drop samples from the photometric probability distributions. As above, we find negligible contamination at the brighter magnitudes. Combining sources with UV luminosities spanning $-20 \lesssim M_{\rm UV} \lesssim -18$, we find that the contamination fraction increases from 2 per cent for V and i' drops to 5 per cent for B drops. This suggests that in this luminosity regime, the B-drop Lyα fraction will be underestimated by a factor of 1.05, while the V- and i'-drop Lyα fraction will be underestimated by a factor of 1.02. Hence, low-z contamination will cause the positive evolution in the Lyα fraction with redshift to be overestimated by a factor of 1.03 in this luminosity range. As we will show in Section 4.2, while the redshift-dependent trends in the Lyα fraction are small in their amplitude, this contamination effect contributes little to the observed variation with redshift.

4 ANALYSIS

We now turn to the key questions posed in Section 1. Armed with a large sample of LBGs for which some fraction, $x_{\rm Ly\alpha}$, show Lyα emission, we discuss what can be learned about the demographics of line emission in the star-forming population and how such trends might affect our ability to use Lyα as a tracer of reionization. In this section, we first present the results, both in terms of the fraction of LBGs showing line emission as a function of luminosity and redshift. We then discuss the physical factors that might explain these trends prior to discussing the use of Lyα emission statistics as a possible probe of reionization.

4.1 The luminosity-dependence of Lyα emission at high redshift

First, we discuss the relationship between Lyα emission and luminosity in our spectroscopic sample of LAE between $3 \lesssim z \lesssim 6$. If the Lyα fraction varies strongly with luminosity, as may be expected given recent claims of luminosity-dependent dust obscuration at high redshift (Reddy & Steidel 2009; Bouwens et al. 2009b), then care must be taken to compare only galaxies of similar luminosity when searching for evolution in the Lyα fraction with redshift. As our survey probes to considerably lower luminosities than past spectroscopic LBG samples at $z \gtrsim 3$ ($M_{\rm UV} \simeq -18$; Fig. 6), our sample is well-suited to investigate such a relationship.

There have been a number of previous studies which examine how Lyα line strength varies with luminosity. Many of these studies have reported a correlation between Lyα equivalent width and UV luminosity. Shapley et al. (2003) binned their sample of $z \simeq 3$ galaxies with $W_{\rm Ly\alpha,0} > 20$ Å in three groups of apparent UV luminosity and found that the mean of the $W_{\rm Ly\alpha,0}$ distribution increased towards fainter UV luminosity. Others have examined Lyα equivalent widths as a function of UV continuum luminosity, revealing a deficit in large equivalent width Lyα lines in the most luminous continuum sources (Ando et al. 2006; Ouchi et al. 2008; Pentericci et al. 2009; Vanzella et al. 2009; Balestra et al. 2010). Additionally, by comparing the UV LF of LBGs with that of narrowband-selected LAEs, Ouchi et al. (2008) have shown that LAE are likely to be more prevalent at the faint-end of the LF. As we discussed earlier, these results are consistent with simple theoretical expectations in which low-luminosity galaxies are less obscured by dust (due to lower metallicities) and perhaps have lower column densities (or covering fraction) of H I surrounding them (e.g. Verhamme et al. 2006, 2008; Schaerer & Verhamme 2008). Perhaps of equal or greater importance is the bulk velocity field of the H I (Shapley et al. 2003; Steidel et al. 2010), which we discuss further in Section 4.3.

However, others have found the evidence for a correlation between luminosity and Lyα equivalent width to be less convincing (e.g. Steidel et al. 2000; Nilsson et al. 2009). In particular, Nilsson et al. (2009) demonstrated that the dearth of luminous galaxies with extreme Lyα emission in magnitude or flux-limited surveys does not require the equivalent width distribution to be luminosity-dependent. The lack of such extreme emitters is actually expected in a magnitude or flux-limited survey, as the most luminous and the most extreme emitters are both rare, causing this portion of parameter space to be poorly represented unless very large volumes are covered. This is an important realization but only considers LBGs with continuum luminosities brighter than $M_{\rm UV} \simeq -20$, significantly more luminous than the feeble sources probed in our survey. Likewise, Kornei et al. (2010) found only marginal evidence for a correlation between $W_{\rm Ly\alpha}$ and UV continuum luminosity in a large sample of $z \simeq 3$ LBGs, but concluded that this may result from the limited dynamic range in UV luminosity probed by their sample.

Fig. 12 shows the distribution of rest-frame equivalent width, $W_{\rm Ly\alpha,0}$ for LAE in our survey as a function of rest-frame UV luminosity, $M_{\rm UV}$. In considering this figure, we must choose a sufficiently bright $W_{\rm Ly\alpha,0}$ threshold to avoid incompleteness in the faintest sources. As demonstrated in Section 3.3 and Fig. 11, sources with $W_{\rm Ly\alpha,0}$ in excess of 50 Å are detected with high completeness (>90 per cent) across our spectra, so we adopt this value as our equivalent width threshold. The data show an apparent lack of strong line emission among the most luminous dropouts, as has been found elsewhere (Ando et al. 2006; Pentericci et al. 2009; Vanzella et al. 2009), yet as demonstrated in Nilsson et al. (2009), this does not necessarily imply that Lyα emission is less common in luminous galaxies. However, when Fig. 12 is viewed in concert with the absolute magnitude histogram of our spectroscopic sample (Fig. 6), it becomes clear that strong line emission must be more common in low-luminosity dropouts, for the number of low-luminosity galaxies ($M_{\rm UV} > -19.5$) targeted in our campaign is as low as the most luminous sources ($M_{\rm UV} < -21.5$), but the number of strong line emitters is far greater among the feeble sources. We emphasize that owing to our equivalent width threshold of $W_{\rm Ly\alpha,0} \simeq 50$ Å, the LAEs amongst low-luminosity sources are secure and robust (S/N > 10)

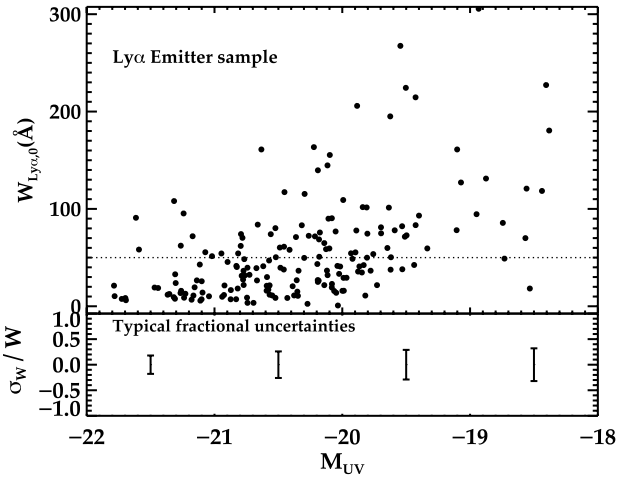

Figure 12. Rest-frame Lyα equivalent width ($W_{Lyα,0}$) as a function of rest-frame absolute magnitude, M_{UV} for LAEs in our spectroscopic sample. The sample is nearly complete at all M_{UV} for sources with $W_{Lyα,0} > 50$ Å (dotted line). For very faint sources (e.g. $M_{UV} \simeq -20$), this equivalent width limit corresponds roughly to the 10σ line flux sensitivity, explaining the dearth of sources below the dashed line at low luminosity. In the bottom panel, we illustrate the typical uncertainty in the equivalent widths as a function of rest-UV absolute magnitude, including the systematic uncertainty discussed in Fig. 10.

detections (similar to those at the top of Fig. 1); hence this result is not driven by noisy features.

In order to most clearly quantify the luminosity-dependence of Lyα emission, we must compute the *fraction of LBGs in our spectroscopic sample that show strong Lyα emission*, $x_{Lyα}$, as a function of emerging UV luminosity. Given that the majority of our spectroscopic sample is fainter than our continuum flux sensitivity (Fig. 5), it is not possible to measure redshifts for faint sources without emission. Hence, if we were to compute $x_{Lyα}$ based solely on sources with confirmed redshifts (as has been done previously for brighter samples), we would artificially increase $x_{Lyα}$ towards lower luminosities. To avoid this bias, we define $x_{Lyα}$ as the number of LAE above some $W_{Lyα,0}$ threshold divided by the total number of dropouts placed on our slitmasks.

The error on $x_{Lyα}$ is computed as follows. We first derive the Poisson error from the number of sources considered in each luminosity or redshift bin. In addition to the Poisson error, each measurement is subject to additional error owing to uncertainty in the equivalent width measurements. We thus conduct Monte Carlo simulations, randomly varying the equivalent width of each galaxy assuming a normal distribution with mean and standard deviation corresponding to the measured $W_{Lyα,0}$ and σ_W. For each realization, we compute the luminosity-dependent Lyα fraction. Considering all the trials, we compute the standard deviation in the $x_{Lyα}$ distribution. We then combine this error term in quadrature with the random error derived above. In doing these simulations, we also consider whether equivalent width error may artificially scatter a net flux of feeble galaxies above our equivalent width threshold, introducing the observed trend. However, the simulations demonstrate that this is not the case, as the trend is readily apparent in each realization.

In constructing the Lyα fraction, we must also recognize that the wavelength coverage of some spectra is such that Lyα would not be recovered across the full redshift range over which those dropouts might be selected. This applies mostly to FORS2 spectra of *B* drops which can only detect Lyα for sources with $z \gtrsim 3.9$. Given that *B* drops are expected to span the redshift range $3.5 \lesssim z \lesssim 4.5$, this suggests that a large number of *B* drops would not be recovered in the FORS2 spectra even if they showed Lyα in emission. We therefore limit our study of *B* drops to those with spectra that allow Lyα to be detected over the entire redshift range expected. This is a particular advantage of the DEIMOS component of our survey where the numerous *B* drops taken with the 600 line mm^{-1} grating are fully sampled.

Following this procedure, we compute the luminosity-dependence of our entire spectroscopic sample. We find that $x_{Lyα}$ is considerably larger in low-luminosity LBGs (Fig. 13), increasing from 10–20 per cent for luminous sources ($M_{UV} \simeq -21$) to 60–70 per cent for feeble galaxies ($M_{UV} \simeq -18$ –19). A similar trend is seen if we adopt larger equivalent width thresholds. With our current data and errors, we can reject the hypothesis of no dependence between $x_{Lyα}$ and M_{UV} with >99.9 per cent confidence. Looking at Fig. 13, we see that the Lyα fraction rises slowly with decreasing luminosity over $-22.0 \lesssim M_{UV} \lesssim -20.5$ but then begins to increase more rapidly at lower luminosities ($-20.5 \lesssim M_{UV} \lesssim -18.5$). We thus choose to fit first-order polynomials over each of these luminosity ranges, finding $x_{Lyα} = 1.09 + 0.047\,M_{UV}$ at the luminous end and $x_{Lyα} = 5.46 + 0.26\,M_{UV}$ for the lower luminosity sources. But we note that owing to the considerable uncertainties in the Lyα fraction at low luminosity, we cannot formally rule out a single slope fit to the data across all luminosities ($x_{Lyα} = 2.10 + 0.096\,M_{UV}$). Improved Lyα statistics at the faint end of the LF are required to confirm or reject the existence of a more complex fit to the data. However, regardless of the precise form of the fit, the addition of Lyα measurements at low continuum luminosities requires models that produce larger Lyα fractions for feeble sources than would have been predicted from extrapolating measurements of Lyα statistics in more luminous sources. Indeed, given that the Lyα fraction increases slowly with decreasing luminosity for luminous sources, it is perhaps no surprise that previous studies which were limited to this luminosity regime found only moderate evidence for luminosity-dependent trends (Nilsson et al. 2009; Kornei et al. 2010); it is only by probing lower luminosity galaxies that we start to see a clear trend in the prevalence of Lyα with luminosity.

In order to put these results in context, it is interesting to estimate the escape fraction of Lyα photons that is implied by these large equivalent widths. In particular, we are interested in the Lyα escape fraction that is implied by the $W_{Lyα,0} \simeq 50$ Å threshold we have adopted. Assuming a Salpeter IMF with $M_{upper} = 120\,M_\odot$, case B recombination, constant star formation and metallicity ranging between $Z = 1/20\,Z_\odot$ and $Z_\odot$, Lyα equivalent widths can be as high as ≃200–300 Å in the first few Myr of the star formation episode, asymptoting to ≃100 Å after 10 Myr (Malhotra & Rhoads 2002; Schaerer 2003). Hence our equivalent width threshold corresponds to a Lyα escape fraction of 15–50 per cent. Of course, this assumes that all ionising photons are absorbed; if there is significant Lyman continuum leakage, then the predicted equivalent widths would decrease, increasing the inferred Lyα escape fraction. Alternatively, if dust is confined to cold neutral clouds, then the maximum Lyα equivalent widths may be larger than quoted above (Neufeld 1991; Hansen & Oh 2006; Finkelstein et al. 2008), decreasing the implied Lyα escape fraction.

These results provide clear evidence that Lyα emission becomes continuously more prevalent among lower luminosity star-forming galaxies. Indeed, it appears that the *majority* of feeble ($M_{UV} < -19$) sources are strong LAE. These results appear to indicate that the escape fraction of Lyα photons (relative to that of far-UV continuum photons) is strongly luminosity-dependent and at very

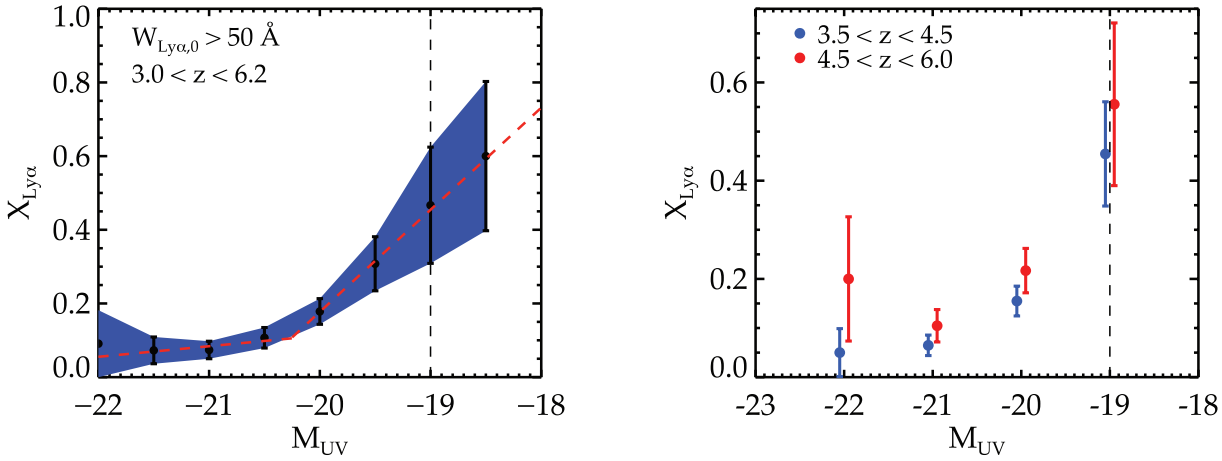

Figure 13. Left: fraction of spectroscopic dropout sample showing strong Lyα emission ($W_{\mathrm{Ly}\alpha,0} > 50$ Å) as a function of UV luminosity. The dashed lines correspond to the first-order polynomial fits to the Lyα fractions in the range $-22.0 \lesssim M_{\mathrm{UV}} \lesssim -20.5$ and $-20.0 \lesssim M_{\mathrm{UV}} \lesssim -18.5$. Right: fraction of spectroscopic dropout sample showing strong Lyα emission ($W_{\mathrm{Ly}\alpha} > 50$ Å) as a function of UV luminosity for samples with $3.5 < z < 4.5$ (blue circles) and $4.5 < z < 6.0$ (red circles). Vertical lines correspond to $\simeq$90 per cent completeness limits for *B*- and *V*-drop samples. For the i' drops, the completeness limits are $\simeq$0.7 mag brighter. Any incompleteness would serve to increase the Lyα fractions further.

low continuum luminosities may commonly exceed the 5 per cent robustly derived (at $z \simeq 2$) via Lyα and Hα surveys (Hayes et al. 2010). In the following section, we determine whether the Lyα fraction changes with redshift, and in Section 4.3 we examine the physical mechanisms which govern the observed Lyα trends.

4.2 Variation in the Lyα fraction in the redshift range $3 \lesssim z \lesssim 6$

We now examine the redshift evolution of the prevalence of LAE in the LBG population over $3 < z < 6$. Since the IGM appears to be highly ionized over this redshift range, this measurement provides the opportunity to understand the extent to which factors other than IGM attenuation affect the Lyα fraction. By calibrating these effects over this redshift interval, we can more accurately detect the signal of reionization on the Lyα fraction.

We consider luminosity-dependent samples in two separate redshift bins, $3.0 < z < 4.5$ and $4.5 < z < 6.0$ (Fig. 13). Sources without spectroscopic redshifts are placed into one bin or the other based on their photometric redshift (see Stark et al. 2009 for discussion of photometric redshifts). In each UV luminosity bin, the fraction $x_{\mathrm{Ly}\alpha}$ increases with redshift. The two bins with the lowest error and incompleteness ($M_{\mathrm{UV}} \simeq -21$ and -20) show increases of 60 and 40 per cent, respectively. Our equivalent width threshold and redshift binning ensure that this result is not biased by redshift-dependent incompleteness. To determine the differential growth, we compute the average change in Lyα fraction, $\Delta x_{\mathrm{Ly}\alpha}$, across all luminosity bins (weighted by the inverse variance of each bin) and compute Δz using the median redshift in each of the two bins. With this approach, we find that the Lyα fraction increases with redshift following $\mathrm{d}x_{\mathrm{Ly}\alpha}/\mathrm{d}z \simeq 0.05 \pm 0.03$. Applying the best-fitting model of $x_{\mathrm{Ly}\alpha}(M_{\mathrm{UV}})$ at $3.5 < z < 4.5$ (blue points in Fig. 13b) to the measured $x_{\mathrm{Ly}\alpha}(M_{\mathrm{UV}})$ $4.5 < z < 6.0$ (red points in Fig. 13b), we find a poorer fit ($\Delta\chi^2 = 3$) to the higher redshift data. Clearly, additional data are required to improve the statistical reliability of the observed redshift evolution. As we mentioned in Section 3.4, low-z contamination appears to decrease very slightly with redshift. However, we find that this effect introduces such small changes in the Lyα fractions ($\lesssim$1 per cent) in each redshift bin, such that the weighted Lyα fraction redshift evolution remains as quoted above. Hence, Lyα fractions grow by nearly $\Delta x_{\mathrm{Ly}\alpha} \simeq 0.1 \pm 0.06$ at fixed M_{UV} between $z \simeq 4$ and $z \simeq 6$.

We emphasize that this trend is not driven by biases associated with LBG selection. It is well-established that the presence of strong Lyα can affect the broad-band colours used for dropout selection (Stanway et al. 2007; Stanway, Bremer & Lehnert 2008). Line emission can either boost the dropout colour (if the redshift is at the high end of the distribution with Lyα in the redder filter) or dilute the colour (if the redshift is at the low end with Lyα in the bluer filter). In principle, this could lead to Lyα being preferentially recovered at higher redshifts. But we minimize these biases by simultaneously targeting the *B*-, *V*- and i'-dropout population. For example, sources with very strong Lyα emission at $5.5 < z < 5.7$ (such that the line falls in the i'_{775}-band) may be scattered out of the i'-drop selection but would instead appear in *V* drop selections. Thus, in this case, by conducting spectroscopy of *V* drops, we can account for this diffusion of Lyα sources. Similarly, our *B* drop sample will contain the small number of sources at $4.5 < z < 4.8$ with very high strong Lyα contaminating the V_{606}-band filter (which would otherwise have little flux). While we do not target *U* drops, Lyα emission from galaxies at $3.5 < z < 3.8$ does not contaminate the B_{435}-band filter, so our *B* drop sample should not have redshift-dependent biases.

The redshift dependence of $x_{\mathrm{Ly}\alpha}$ is affected not only by evolution in the internal properties of galaxies but also by the increase in the density of the IGM with redshift. At $z \simeq 6$, the IGM provides a significantly greater optical depth to Lyα photons than that at $z \simeq 4$, resulting in a second-order effect on the Lyα fraction. In the absence of IGM density evolution, we would thus expect the redshift evolution of the Lyα fraction to be slightly greater than derived above. We can attempt to estimate the variation in $x_{\mathrm{Ly}\alpha}$ that is intrinsic to *galaxy evolution* (e.g. dust, ISM kinematics) by subtracting the differential evolution expected from changes in IGM density. Deconvolving the effects of the IGM on Lyα radiative transfer requires careful modelling of the local density, velocity and ionization field (e.g. Santos 2004; Dijkstra, Lidz & Wyithe 2007a; Dijkstra, Wyithe & Haiman 2007b; Zheng et al. 2010). We delay such a treatment to subsequent works, and instead we follow a very simple approach adopted in Ouchi et al. (2008) which yields a very rough estimate of the intrinsic redshift evolution of the Lyα

fraction. We compute the percentage of photons absorbed by the IGM assuming that the blue side of the Lyα line is attenuated by exp $[\tau_\alpha(z)]$, where $\tau_\alpha(z)$ is the optical depth for Lyα photons as computed in Meiksin (2006). With this approach, we find that the IGM absorbs 28, 42 and 49 per cent of the Lyα line flux at $z \simeq 4$, 5 and 6. In a more sophisticated and realistic treatment, the density and ionising background surrounding LAEs is likely to be greater than the mean, and infalling gas would also erase a fraction of the Lyα line redwards of rest frame 1216 Å; the combination of these effects can cause the redshift evolution in the transmission of Lyα photons through a reionized IGM to be considerably different than implied by our model given above (e.g. Santos 2004; Dijkstra et al. 2007b). We will model this effect in greater detail in the future. For the sake of clarity, here we define the intrinsic rest-frame equivalent width that would have been observed in the absence of IGM attenuation $W_{\mathrm{Ly}\alpha,0,\mathrm{int}}$, where the IGM absorption is taken to follow the numbers derived above. Adopting a fixed intrinsic $W_{\mathrm{Ly}\alpha,0,\mathrm{int}}$, we derive Lyα fractions as above and find that the differential redshift evolution in $x_{\mathrm{Ly}\alpha}$ increases to $\mathrm{d}x_{\mathrm{Ly}\alpha}/\mathrm{d}z \simeq 0.12 \pm 0.07$. In the next section, we attempt to understand the factors likely to be creating this redshift trend and the luminosity trend presented in the previous section.

4.3 The factors governing the Lyα escape fraction

Earlier we demonstrated that prevalence of strong Lyα emission increases towards lower luminosities and higher redshifts. Here, we discuss the factors that are likely governing the observed trends prior to exploring the use of higher redshift galaxies and their line emission as a probe of cosmic reionization. In Section 4.3.1, we examine whether trends in dust obscuration could potentially drive the observed Lyα fraction relations. In Sections 4.3.2 and 4.3.3, we discuss how the geometric distribution and kinematics of the surrounding ISM may impact the Lyα fraction trends we observe and discuss future spectroscopic work in progress to provide further insight into the ISM of feeble high-z galaxies. Finally in Sections 4.3.4 and 4.3.5, we close our discussion with a variety of factors possibly affecting Lyα that are more difficult to directly constrain observationally.

4.3.1 Impact of dust extinction

Previous observations have demonstrated that, among luminous LBGs, those objects showing Lyα in emission tend to display bluer UV continuum slopes than those with Lyα absorption (Shapley et al. 2001, 2003; Vanzella et al. 2009; Pentericci et al. 2009; Kornei et al. 2010). While the presence of dust may enhance Lyα relative to the continuum (Neufeld 1991; Hansen & Oh 2006; Finkelstein et al. 2008), the results in Fig. 14 suggest that most often, the presence of significant quantities of dust generally leads to increased absorption of Lyα photons relative to the continuum.

Here, we examine whether similar trends are seen at lower luminosities. In order not to bias the UV colours, we determine the slopes using filters that are not contaminated with Lyα emission or IGM absorption. Obtaining accurate UV slopes requires very accurate colour measurements, thus we choose to focus on the *B* drops, as the UV colours can be determined entirely from deep i'- and z-band imaging with ACS. We translate the UV colours into UV slopes using the relation presented in Bouwens et al. (2009b): $\beta = 5.30(i_{775} - z_{850})$–2.04. We have verified that this relation holds for a variety of star formation histories and age combinations that are appropriate for the $z \simeq 4$–6 population.

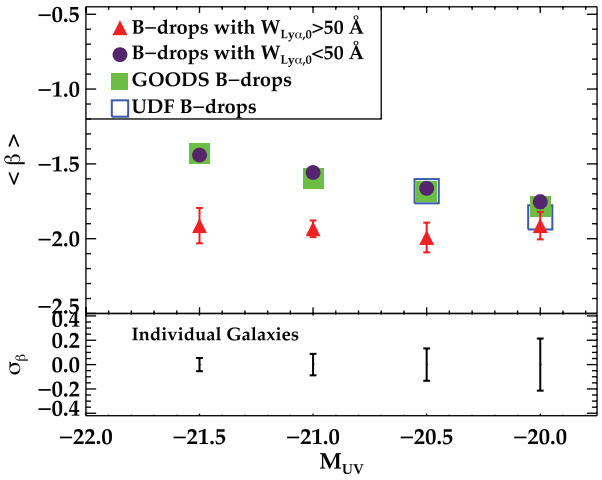

Figure 14. Average UV slopes of *B* drops with and without strong Lyα emission. Average UV slopes of *B* drops (grouped in bins of M_{UV}) from the spectroscopic sample with strong Lyα emission ($W_{\mathrm{Ly}\alpha} > 50$ Å) are denoted by red triangles, while the average UV slopes rest of the *B*-drop sample is denoted by purple circles. For reference, we overplot the average UV slope as a function of M_{UV} for the entire photometric sample of *B* drops in GOODS-N and GOODS-S from Stark et al. (2009) as filled green squares. The average UV slope from *B* drops in the Hubble UDF is shown as open blue squares. Typical uncertainties in the UV slopes of individual galaxies are shown as error bars on the bottom of the plot; uncertainties in the mean take both this error and the number of sources in each bin into account. Owing to biases in the selection of LBGs, converting the measured mean UV slopes presented here to those intrinsic to the population requires a redwards shift of $\Delta\beta \simeq 0.1$ (see Bouwens et al. 2009b).

Given the relationship between UV colour and β, it is important to note that even a small photometric colour error translates into substantial uncertainty in the derived UV slope. We thus estimate the luminosity limit at which the GOODS data become unreliable for estimating UV slopes by comparing the average UV slopes of *B* drops in GOODS with UV slope measurements from higher S/N data in the UDF, using the photometric catalogues of Coe et al. (2006) for our UDF sample. These results indicate that UV slopes measured from the GOODS data set differ significantly from those determined from the high S/N UDF sample for *B* drops with luminosities fainter than $M_{\mathrm{UV}} \simeq -20.5$. Therefore, we cannot derive robust UV slopes for sources in our GOODS spectroscopic sample that are fainter than this limit.

Concentrating on the brighter subset of objects, we examine the UV slopes of our *B*-drop spectroscopic sample as a function of UV luminosity (Fig. 14). The data show that galaxies with strong Lyα in emission ($W_{\mathrm{Ly}\alpha,0} > 50$ Å) are bluer than those systems without strong Lyα emission, and are generally fit with $\beta = -2.0$ across the entire luminosity range covered. Following Meurer, Heckman & Calzetti (1999), this value is consistent with very little dust obscuration ($A_{1600} \simeq 0.5$), assuming a Calzetti extinction curve and normal stellar populations. The UV slopes of the overall population of *B* drops are significantly redder than the LAEs, but when viewed as a function of luminosity, they grow steadily bluer towards low luminosities, ranging from $\langle\beta\rangle \simeq -1.4$ (at $M_{\mathrm{UV}} \simeq -21.5$) to $\langle\beta\rangle \simeq -1.7$ (at $M_{\mathrm{UV}} \simeq -20.5$). We note that these values correspond to the *measured* mean of the UV slope distribution. It has been shown in Bouwens et al. (2009b) that there is a small selection bias that alters the measured UV colour distribution from the intrinsic distribution of the population by $\Delta\beta \simeq 0.1$ owing to the fact that the selection volume for bluer LBGs is slightly larger than that for redder LBGs.

Simulations from Bouwens et al. (2009b) suggest that the amplitude of this shift does not vary significantly with absolute rest-UV magnitude in the range considered in our paper, so the measured slope in Fig. 14 should be very close to the slope of the intrinsic distribution.

The correlation between UV slope and emerging UV luminosity at these redshifts was first demonstrated in a large photometric sample in Bouwens et al. (2009b); here we confirm this trend with a spectroscopic sample of dropouts. As argued in Bouwens et al. (2009b), the trend most likely arises as a result of lower luminosity galaxies having less dust obscuration. While changes in the mean age, metallicity and stellar IMF do also affect the mean UV slope, changes in the mean dust content have a stronger effect. Specifically, Bouwens et al. (2009b) showed that a factor of 2 change in the age and metallicity alters the UV continuum slope β by $\simeq$0.1 and $\simeq$0.05, while the same factor of 2 change in the mean dust content changes the mean UV slope by $\simeq$0.35. While these results suggest that changes in the age distribution could play a non-negligible role in any observed shift in the UV slope distribution, our previous work suggests that, at least in the UV luminosity and redshift range covered in our current survey, the median ages of LBGs do not vary significantly with redshift or luminosity. Hence the observed shift in the UV slope distribution is most likely driven by luminosity-dependent dust obscuration.

Given that strong LAEs tend to arise in galaxies with blue UV slopes (and thus little dust extinction), it is perhaps no surprise that we see a larger Lyα fraction in low-luminosity galaxies. Similar reasoning can also explain the observed redshift-dependence of the Lyα fraction, as UV slopes are found to grow steadily bluer with redshift over $3 \lesssim z \lesssim 6$ (Bouwens et al. 2009b).

If we attribute the luminosity-dependence of the Lyα fraction to the variation in dust obscuration, we can derive a relationship between mean UV slope and Lyα fraction. From Fig. 14, we find that $\mathrm{d}\beta/\mathrm{d}M_{\mathrm{UV}} \simeq -0.23 \pm 0.15$ over $-21.5 < M_{\mathrm{UV}} < -20.0$. Using data from the UDF and GOODS, Bouwens et al. (2009b) have shown that a similar $\mathrm{d}\beta/\mathrm{d}M_{\mathrm{UV}}$ applies at lower continuum luminosities. Averaged over the entire luminosity range probed by our spectroscopic observations, we find that the Lyα fraction, $x_{\mathrm{Ly}\alpha}$ varies with UV luminosity as $\mathrm{d}x_{\mathrm{Ly}\alpha}/\mathrm{d}M_{\mathrm{UV}} = 0.13 \pm 0.058$. Assuming that dust extinction drives the evolution in the Lyα fraction, we derive $\mathrm{d}x_{\mathrm{Ly}\alpha}/\mathrm{d}\beta = -0.57 \pm 0.16$. While this result was derived from the luminosity-dependence of $x_{\mathrm{Ly}\alpha}$, it should also apply to the redshift evolution if dust obscuration were to dominate the redshift-dependent trends. Measurements of similarly luminous $z \simeq 6$ LBGs (Bouwens et al. 2009b) suggest that the average UV slopes grow bluer by $\Delta\beta \simeq -0.64 \pm 0.21$ from $z \simeq 4$ to $z \simeq 6$. If dust evolution dominates the redshift-dependence of the Lyα fraction and the evolution in UV slopes, the above relationship suggests that $x_{\mathrm{Ly}\alpha}$ should increase by $\Delta x_{\mathrm{Ly}\alpha} = 0.36 \pm 0.26$. The fact that the actual redshift evolution is marginally less rapid ($\Delta x_{\mathrm{Ly}\alpha} = 0.24 \pm 0.14$ after roughly accounting for IGM absorption) is not surprising given the uncertainties. Several other factors likely contribute to the small discrepancy. For example, it is likely that the luminosity dependence of $x_{\mathrm{Ly}\alpha}$ is driven by more than just dust obscuration (see the following sections for a discussion). Additionally, as UV slopes grow bluer than $\beta = -2.0$, the variation in the UV slope is possibly driven by factors other than dust obscuration (e.g. Stanway et al. 2005; Bouwens et al. 2010a). Secondly, given that $x_{\mathrm{Ly}\alpha}$ cannot be larger than 1.0, the differential growth must slow down as $x_{\mathrm{Ly}\alpha}$ increases; hence any extrapolation of the $x_{\mathrm{Ly}\alpha}$ relations below our completeness limits is highly uncertain. Finally, as emphasized in Section 4.2, our simple treatment of IGM absorption may incorrectly estimate the evolution in the Lyα fraction that is intrinsic to galaxy processes.

In summary, these results indicate that the variation in dust extinction with luminosity and redshift likely plays an important role in governing the observed evolution and luminosity-dependence in the Lyα fractions. But, not surprisingly, it seems likely that additional factors play a role in governing $x_{\mathrm{Ly}\alpha}$ as well. We discuss these in more detail below.

4.3.2 The hydrogen covering fraction

After Lyα photons escape the H II regions where they were created, they must diffuse through neutral gas and dust at larger radii. This could include gas that is participating in outflows surrounding the galaxy in addition to gas that is being accreted on to the galaxies. Rest-UV spectra of high-redshift star-forming galaxies reveal low-ionization absorption lines that are generally blueshifted by $\Delta v \simeq -200$ km s^{-1} (Shapley et al. 2003; Steidel et al. 2010) relative to the centre of rest, indicating that outflowing neutral gas is nearly always present, while accreting gas appears less prevalent. The geometrical distribution and kinematics of this outflowing material play a crucial role in governing the escape of Lyα photons. This is clearly evidenced by the fact that Lyα photons are typically observed to be redshifted by $\simeq$400–500 km s^{-1} with respect to the centre of rest (Steidel et al. 2010). This result implies that the majority of Lyα photons to escape through the absorbing material along the line of sight are those that achieve a sufficient (redshifted) velocity such that they can travel through the intervening material without resonantly scattering. This is most easily accomplished in a model in which the Lyα photons that are observed are those that have been 'backscattered' off of the outflowing material on the far side of the galaxy (e.g. Shapley et al. 2003; Steidel et al. 2010). Hence, it is likely that the increased prevalence of LAE among low-luminosity galaxies tells us something about the distribution and/or kinematics of the ISM of feeble sources. In this section, we discuss the relationship of the ISM distribution, dust obscuration and Lyα emission in luminous LBGs as found in the previous work, and then consider whether a similar picture is likely to hold for low-luminosity galaxies; in the following section, we focus on the kinematics of the ISM.

Even for luminous sources, observational constraints on the distribution of the blueshifted neutral absorbing gas in the immediate vicinity of high redshift galaxies are limited. The spectroscopic study of $z \simeq 3$ LBGs conducted in Shapley et al. (2003) revealed a strong correlation between the equivalent width of low-ionization interstellar absorption lines (W_{LIS}) and that of Lyα, in the sense that the strongest LAE tend to have the least absorption by the low-ionization ISM. As the absorption lines are highly saturated, Shapley et al. (2003) note that the trend in W_{LIS} is due to either variations in the velocity width or the covering fraction of absorbing gas, with the latter argued to be the dominant factor, such that sources showing strong Lyα emission, on average, have the patchiest distribution of absorbing gas covering the continuum source (at least along the line of sight). Galaxies also show a strong correlation between W_{LIS} and $E(B-V)$, which Shapley et al. (2003) argue implies a significant fraction of the dust which reddens the stellar continuum (and absorbs Lyα photons) located *within* the outflowing neutral gas. As noted in Steidel et al. (2010), from a theoretical standpoint, the exact effect of a non-uniform covering fraction on the observed Lyα flux is not obvious. But regardless, these observations thus suggest a scenario in which strong Lyα emission is generally coupled with low dust extinction and a low hydrogen covering fraction, a picture

supported by recent observations of strongly lensed LBGs at $z \simeq 3$ (Quider et al. 2009, 2010) for which direct measures of the covering fractions of various ions are available.

If similar trends are present in low-luminosity galaxies, then the fact that Lyα is much more common in feeble galaxies may imply that these sources typically have lower covering fractions of absorbing gas than more luminous LBGs. Addressing whether this is indeed the case requires deep spectroscopy of UV-faint systems, and thus is perhaps only feasible via studies of gravitationally lensed galaxies. Some progress can be made with current field samples however. In particular, we can determine whether the coupling between strong LAE and weak ISM absorption is also present for feeble galaxies by creating composite spectra of LAE binned by $M_{\rm UV}$. We will present the results of this analysis in a subsequent paper (Stark et al. 2010, in preparation). Some indication that the correlation is in place at low intrinsic luminosities is already apparent from the i'-drop composite spectra presented in Vanzella et al. (2009). As all the i' drops in their sample are UV faint ($<M_{\rm UV}> \simeq -20$), this spectrum provides insight into the properties of feeble sources. Owing to the faintness of the i' drops, the composite is dominated by strong LAE and shows very weak interstellar absorption lines. Higher S/N spectra are required to ensure that the absorption lines are saturated and to quantify the absorption line equivalent widths.

Finally, while admittedly speculative, we note briefly that if a low hydrogen covering fraction is more common for low-luminosity galaxies, it may also enable Lyman continuum photons to more easily escape from feeble systems. Naively, this statement seems contradictory since the presence of Lyα photons stems from the absorption of ionising photons. However, high-redshift galaxies are clearly not perfect H II regions. In practice, a significant fraction of ionising photons are absorbed in the ionized regions surrounding the massive stars, leading to the production of Lyα photons. Both Lyα photons and any escaping ionising photons will then approach the surrounding neutral ISM, much of which is likely moving at great speeds with respect to the stars. Clearly, those systems with significant holes in their surrounding distribution of hydrogen will leak a larger fraction of ionising radiation. Indeed, the combination of strong Lyα and significant ionising photon escape fractions are seen in observations at $z \simeq 2$ (Shapley et al. 2006). Intriguingly, recent results reveal a possible trend toward greater Lyman continuum leakage in sources with low UV continuum luminosities (Steidel et al., in preparation). While much work is still required to verify the luminosity-dependence in the hydrogen covering fraction and the Lyman continuum escape fraction, these results strongly motivate detailed study of the physical properties of low-luminosity galaxies.

4.3.3 Kinematics of ISM

As we discussed above, Lyα is affected not only by the geometry and column density of the dust and hydrogen around it but also by the velocity distribution of the surrounding neutral H I. Recently, Steidel et al. (2010) have compared the kinematics of the absorbing gas (extracted from the properties of rest-UV absorption lines) and the properties of Lyα as a function of total baryon mass for a sample of $z \simeq 2$ UV continuum-selected galaxies. These results reveal that the low-mass subset shows significantly stronger Lyα emission, as we would expect from Fig. 13, on the assumption that the feeble sources that we have studied spectroscopically are generally lower mass systems. Steidel et al. (2010) demonstrate that the absorbing medium is significantly different for these two mass subsets, with the more massive galaxies more often having a significant component of interstellar absorption at velocities close to the systemic redshift (and often extending to positive velocities). These high-mass systems not only have weaker Lyα emission but the redshifted velocity of Lyα is greater than in low-mass galaxies. The nature of this excess absorption component at zero velocity for massive galaxies is unclear; as discussed in detail in Steidel et al. (2010) it could possibly be outflowing material which has stalled due perhaps to the larger gravitational potential, or alternatively infalling gas.

Regardless, it is clear that there are significant mass-dependent variations in the kinematics of the absorbing gas, particularly at $v = 0$, such that lower mass galaxies transmit a larger fraction of their Lyα photons to the Earth. These trends, together with those seen in dust obscuration and perhaps hydrogen covering fraction, may play a large role in governing the luminosity-dependence of the Lyα fraction seen in Fig. 13. Future spectroscopic work of feeble galaxies which are magnified via gravitational lensing can help confirm these mass-dependent trends in the ISM kinematics.

4.3.4 Additional factors governing the Lyα fraction

We conclude by mentioning several additional factors which may contribute to the observed Lyα fraction trends. First, the Lyα equivalent width is highest in the earliest stages of star formation (Charlot & Fall 1993; Leitherer et al. 1999), when the contribution from massive, young stars is at its greatest. Studies of UV faint narrowband LAEs have generally shown that these sources have younger ages and higher specific star formation rates than more luminous LBGs (e.g. Pirzkal et al. 2007; Ono et al. 2010). However, a recent study of spectroscopically confirmed LBGs has demonstrated that those sources with strong Lyα emission tend to be older than those without Lyα emission at similar UV luminosities (Shapley et al. 2001; Kornei et al. 2010), leading the authors to suggest a physical picture whereby Lyα emission escapes more easily once large-scale outflows have had time to reduce the dust covering fraction sufficiently. The sample presented in this paper allows us to extend the work of Kornei et al. (2010) to lower continuum luminosities, which we plan to present in a future study (Stark et al. 2010, in preparation), taking care to account for the possible contribution of nebular emission lines to the mid-IR flux (e.g. Schaerer & de Barros 2009).

Additionally, Lyα equivalent width becomes larger at low metallicities owing to the increased ionising flux and harder UV spectra (e.g. Schaerer 2003). Thus, if low-luminosity galaxies have much lower metallicities than luminous systems, then we may expect to see an increased fraction of strong line emitters among UV faint systems. Only via future direct measurements of the metallicity of low-luminosity galaxies at these redshifts will we be able to predict the magnitude of this effect on the luminosity dependence of the Lyα fraction.

Finally, it is, in principle, conceivable that the trends could be driven by variation in the stellar IMF with luminosity and redshift. As has been demonstrated in previous studies (Schaerer 2003), top-heavy IMFs can boost the equivalent widths of Lyα relative to that expected for normal stellar populations. While several studies have argued that the IMF may vary with redshift (e.g. Davé 2008), there is little direct evidence of such a variation.

4.4 Comparison with narrowband Lyα emitter studies

Finally, we compare our results to those determined from studies of narrowband-selected LAEs in the same redshift range (e.g. Shimasaku et al. 2006; Kashikawa et al. 2006; Ouchi et al.

2008). We first contrast the two samples and examine whether the large fraction of strong Lyα emission seen among our UV faint dropouts is consistent with the independently determined LFs of LAEs. Then we consider whether we can use the Lyα trends discovered in our UV continuum samples to explain the lack of redshift evolution in the LFs of the LAE population, which contrasts markedly with the strong evolution seen in the LBG samples.

It is commonly asserted that narrowband LAE samples are fainter than UV continuum LBG samples. While this is true if one compares the LAE samples to the well-studied spectroscopic $z \simeq 3$ population (e.g. Shapley et al. 2001, 2003), current photometric LBG samples extend to much fainter UV luminosities (e.g. $M_{\rm UV} \simeq -16$ at $z \simeq 4$ in the Ultra Deep Field), and as we have discussed above, our spectroscopic observations take advantage of these faint samples, extending to $M_{\rm UV} \simeq -18$ (Fig. 2). Many LAEs identified in typical ground-based surveys are below the UV continuum magnitude limits and require stacking to determine the typical continuum luminosity. In a recent analysis of a large sample of $z = 3.1$ LAEs, Ono et al. (2010) have shown that the stacked continuum magnitude is $i' \simeq 27$, corresponding to $M_{\rm UV} \simeq -18.6$, comparable to the UV continuum luminosity of the faintest galaxies in our spectroscopic sample. Thus, by probing down the LBG LF in our DEIMOS survey, we are able to directly compare the Lyα trends discovered in both populations.

Consider the percentage of LBGs at a given redshift that show strong Lyα emission. Assuming that LBGs form the parent population of LAEs, we can compute the expected number density of strong LAEs as a function of $M_{\rm UV}$. Our spectroscopic data suggest that 8.5 ± 2.3 per cent of B drops with $M_{\rm UV} \simeq -20.5$ show Lyα emission with $W_{{\rm Ly}\alpha,0} > 50$ Å. Based on the number density of LBGs in this luminosity range, these data predict that the density of strong line emitters with $M_{\rm UV} \simeq -20.5$ should be $\simeq 7.4 \pm 2.0 \times 10^{-5}$ Mpc^{-3} mag^{-1}. This value is very similar to the abundance of LAEs in this luminosity range from the UV LFs of narrowband LAEs at $z \simeq 4$ ($8.1 \pm 1.8 \times 10^{-5}$ Mpc^{-3}) (Ouchi et al. 2008). Clearly, this calculation is very uncertain owing to the different selection and equivalent width limits, and is simply meant as a zeroth-order comparison. We note that of the 26 $z = 3.7$ LAEs in Ouchi et al. (2008), 23 have rest-frame equivalent widths greater than our threshold of $\simeq$50 Å, so the LAE sample is not probing significantly further down the equivalent width distribution than our LBG sample. At fainter continuum luminosities ($M_{\rm UV} > -20$), the agreement begins to break down, as our measured Lyα fractions predict a larger abundance of LAEs than inferred from the Ouchi et al. (2008) UV LFs. This is not surprising given that Ouchi et al. (2008) only computed over $-21.7 < M_{\rm UV} < -19.7$ (where the data are sufficiently complete), requiring $M^{\star}_{\rm UV}$ and α to be fixed.

Finally, we consider whether the observed evolution of the Lyα population over $3 \lesssim z \lesssim 6$ is qualitatively consistent with the trends suggested by the luminosity and redshift-dependence of the Lyα fraction. The rapid increase in the Lyα fraction towards lower luminosities suggests that deep narrowband Lyα samples will generally be dominated by UV faint galaxies. Since the redshift evolution of the number density of UV faint LBGs is much less rapid than that of luminous LBGs, we expect the number density of LAEs (which should be weighted more toward UV faint sources) to decrease less rapidly than LBG samples. This trend is enhanced by the increase in the prevalence of Lyα emission in LBGs over this redshift interval. Hence given the luminosity and redshift-dependent trends in the Lyα fraction, it is not necessarily surprising that Ouchi et al. (2008) reveal that the observed Lyα LF does not evolve significantly with redshift over $3.1 < z < 5.7$.

5 IMPLICATIONS FOR REIONIZATION

In the previous section, we showed that strong LAEs become more common between $z \simeq 3$ and $z \simeq 6$. We argued that this trend is likely driven in part by a decrease in dust extinction and the covering fraction of hydrogen surrounding the H II regions where Lyα photons are originally produced. The first estimates of UV slopes at $z \gtrsim 6$ imply that the dust obscuration continues to decline to $z \simeq 7$–8. Given these trends, the expected signal of reionization (decreasing the prevalence of LAEs) should be readily apparent in deep spectroscopy of newly discovered z_{850}-band and Y_{105}-band dropouts (e.g. McLure et al. 2010; Oesch et al. 2010; Bunker et al. 2010; Bouwens et al. 2010a; Wilkins et al. 2010a,b).

Given the increase we find in the Lyα-emitting fraction over $3 \lesssim z \lesssim 6$ (Fig. 13) it is now interesting to examine whether there is any decline seen beyond $z \simeq 6$ such as might arise from an increasing neutral fraction in the IGM. Although our first set of z-drop observations were conducted in poor conditions, we can still provide preliminary constraints on $x_{{\rm Ly}\alpha}$ if we adopt a sufficiently bright equivalent width and magnitude limit. The flux limits from the 2009 October run indicate that detection requires an equivalent width of at least 75 Å (rest frame) for sources in the luminosity bin $-20.5 \lesssim M_{\rm UV} \lesssim -19.5$ (Section 2.1). The Lyα equivalent widths of sources fainter than this limit (all but two of the z drops in the UDF) are not usefully constrained. Also, owing to the increased noise stemming from poor atmospheric conditions it is not possible to detect Lyα with typical equivalent widths in any of the sources studied at redshifts beyond $z \simeq 6.65$. Over the redshift range in which we are sensitive to Lyα emission, completeness simulations indicate that recovery rate of lines with $W_{{\rm Ly}\alpha,0} > 75$ Å is $\simeq$50 $\pm$ 10 per cent. The photometric redshifts derived from the broad-band SEDs indicate that five of the eight z drops are likely to lie at redshifts above $z \simeq 6.65$. If this is true, these objects would escape detection in our DEIMOS spectra. We take this possibility into account in our discussion of the Lyα fractions below.

Fig. 15 shows the overall evolution in the Lyα fraction with redshift within this restricted luminosity range. The fraction of LBGs with Lyα emission above our chosen threshold grows steadily over $4 \lesssim z \lesssim 6$, reaching nearly 20 per cent at $z \simeq 6$. Based on our discussion in the previous section, we argue that this net change likely arises from a combination of the redshift evolution in the dust and hydrogen covering fractions (which increases the Lyα fraction towards higher redshift) and the IGM density (which decreases the Lyα fraction toward higher redshift).

If the line shown in Fig. 8 is Lyα, and if all z drops in our restricted luminosity range ($-20.5 < M_{\rm UV} < -19.5$) lie at $z \lesssim 6.65$ (as is necessary for detection with DEIMOS in the October data set), then our measurements would indicate that the fraction from the October run with $W_{{\rm Ly}\alpha} > 75$ Å (corrected for incompleteness) is marginally greater than that measured at $z \simeq 6$, consistent with the slow increase over $4 < z < 6$. However, given the very large errors in the Lyα fraction, the $z \simeq 6.5$ measurements are also fully consistent with a significant decline over $6.0 < z < 6.5$. However we point out that the measured Lyα fraction may actually be larger than we estimate here, for if five of the z drops are indeed at $z > 6.65$, as suggested by their photometric redshifts, then the Lyα fraction at $z \simeq 6.5$ would be $\simeq 2.6$ times larger than the data point in Fig. 15 indicates. Clearly additional spectroscopy in improved atmospheric conditions is required for robust statements.

Beyond $z \simeq 6.6$, existing data sets imply that the Lyα fraction may begin to decline. In contrast to the abundant samples of robust LBGs now in place at $z \simeq 7$ and beyond (e.g. McLure et al. 2010; Bunker

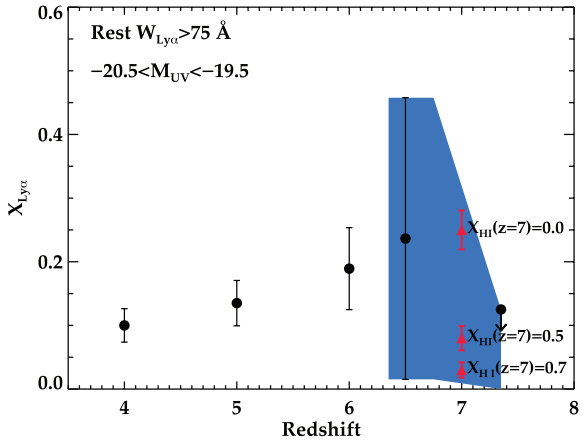

Figure 15. Fraction of spectroscopic dropout sample with $-20.5 < M_{\rm UV} < -19.5$ showing strong Lyα emission ($W_{\rm Ly\alpha} > 75$ Å) over $4 < z < 7$. We estimate the Lyα fraction at $z \simeq 6.5$ from a recent DEIMOS run targeting WFC3 z drops. Owing to poor atmospheric conditions on this run, statistics are insufficient to robustly constrain the evolution in $x_{\rm Ly\alpha}$. However in contrast, the implied Lyα fraction from the lack of Lyα detection in a sample of eight lensed z drops studied with near-IR spectroscopy in Richard et al. (2008) and Kneib et al. (2004) is shown by the upper limit at $z = 7.3$. If these candidates are real and at high redshift, then the implied Lyα fraction at $z \simeq 7$ is lower than measured at $z \simeq 6$. Red triangles and associated errors correspond to measurements that will be possible if a large percentage of z drops expected to be discovered with future observations (e.g. ULTRA-VISTA and WFC3 MCT) are followed up with spectroscopy. The quoted neutral fractions correspond to those implied from a mapping derived from McQuinn et al. (2007) and are only valid at $z \simeq 7$.

et al. 2010; Oesch et al. 2010; Bouwens et al. 2010a), searches for LAEs at $z > 7$ with narrowband filters have yet to reveal a large population of line emitters. While candidates have been identified (e.g. Stark et al. 2007b; Hibon et al. 2010), confirmation has proven challenging. Indeed, the highest redshift LAE with robust spectroscopic verification lies at $z = 6.96$ (Iye et al. 2006). Updated data from this survey (Ota et al. 2008) suggest that the number density of LAEs at $z = 7.0$ is only 17 per cent of that at $z = 6.6$. Attributing this decline in number density to a decrease in Lyα transmission (ignoring the contribution from the declining galaxy number density), we would expect to see strong differential evolution in the Lyα fraction over $6.6 \lesssim z \lesssim 7.0$. In principle, the DEIMOS observations should have easily detected such a decline in the initial sample of 17 z drops observed in 2009 October. Unfortunately, as discussed earlier, the poor conditions prohibit detecting Lyα at $z \gtrsim 6.6$ for the faint sources considered in this work. Therefore we are unable to verify this result with our current DEIMOS data set.

However, the only detailed spectroscopic survey of z drops currently in the literature (Richard et al. 2008) does offer tentative support for the downward trend in the Lyα fraction. In their paper, seven gravitationally lensed z drops were observed with the NIRSPEC spectrograph on Keck (McLean et al. 1998), and none showed evidence for Lyα emission (with rest-frame equivalent width limits as low as ≃30 Å). Likewise, a similar absence of Lyα was seen in the $z \simeq 6.8$ gravitationally lensed galaxy in Abell 2218 (Kneib et al. 2004; Egami et al. 2005). The typical luminosities of these sources are considerably lower than the restricted range used in Fig. 15, hence one would expect them to have Lyα fractions that are significantly greater than those observed at lower redshifts in this figure. In contrast, we measure an upper limit to the $z \simeq 7$ Lyα fraction which is suggestive of a significant decline over $6 < z < 7$. At the very large equivalent width thresholds adopted in this figure, it is unlikely that this decline could be produced by incompleteness owing to the presence of OH emission lines. While these NICMOS dropouts are generally not as robust as the z drops being identified with WFC3 (see Bouwens et al. 2009a), the lack of Lyα is tantalizing in light of the narrowband LAE results (Ota et al. 2008). Such a marked decline in the number density of LAEs should easily be detected in future follow-up of current WFC3 z-drop samples.

We now explore the potential ramifications that these results may have for reionization and discuss the possibility of improving and extending the $x_{\rm Ly\alpha}$ measurements in the future. We first discuss how one may use these measurements to quantify changes in the IGM. Various theoretical studies have examined how an increase in the neutral fraction of the IGM impacts the transmission of Lyα photons (e.g. Santos 2004; Furlanetto et al. 2006; McQuinn et al. 2007; Mesinger & Furlanetto 2008). In this paper, we consider the models of McQuinn et al. (2007), which make use of 200 Mpc radiative transfer simulations to compute the effect of inhomogenous reionization on the transmission of Lyα photons and the clustering of Lyα emitting galaxies. In fig. 4 of their paper, McQuinn et al. (2007) present the Lyα LF at $z = 6.6$ for various H I fractions, ranging from $x_{\rm H\,I} = 0.00$ to $x_{\rm H\,I} = 0.88$. The greater the H I fraction, the more the amplitude of the Lyα LF decreases with respect to the fully ionized case. The relative amplitude of the LFs for various ionization fractions is directly related to the decreased transmission of Lyα photons associated with reionization of the IGM. For example, the amplitude of the Lyα LF decreases by a factor of ≃120 when the H I fraction increases to 0.88.

Our goal is to translate the measured Lyα fractions into estimates of the ionization state of the IGM. We can convert the McQuinn et al. (2007) results into a mapping between Lyα fraction and $x_{\rm H\,I}$ as follows. First, we naively assume that in the absence of any change in the ionization of the IGM, the Lyα fraction would not evolve between $z \simeq 6$ and $z \simeq 7$ (see below for an alternative approach). We then assume that the predicted decline in the amplitude of the Lyα LF (with respect to when the IGM is fully ionized) will result in an identical decrease in the Lyα fraction. Hence if the H I fraction is 0.88 at $z \simeq 7$, we should expect the Lyα fraction to be 120 times lower than its measured value at $z \simeq 6$, when the IGM is ionized. With these assumptions, the current measurements at $z \simeq 6.5$ are consistent with a picture whereby the IGM is still largely ionized (although clearly the errors allow a range of interpretations), while the $z \simeq 7$ upper limit is just at the edge of the 1σ range of our $z \simeq 6$ sample. Larger samples are clearly required for firm statements on $x_{\rm H\,I}$ in this 'no-evolution' scenario.

However given that the Lyα fraction evolves with redshift in the absence of changes in the IGM ionization state, our 'no-evolution' assumption above is clearly simplistic. Indeed, if the dust obscuration continues to evolve over $z \gtrsim 6$–8 (as implied by Bouwens et al. 2010a), then in the absence of IGM ionization state evolution, the Lyα fraction is likely to be even larger at $z \simeq 6.5$–7. If this is the case, then the mapping between Lyα fraction and IGM ionization state discussed above would be incorrect. To account for this, we extend the smooth evolution seen in the Lyα fraction over $4 \lesssim z \lesssim 6$ (when the IGM is highly ionized) to higher redshifts. Following this approach, we would expect to find Lyα fractions (with 75 Å as the lower threshold) of 0.21 ± 0.07 and 0.24 ± 0.08 at $z \simeq 6.5$ and $z \simeq 7.3$, respectively. We adopt these predictions as the baseline $x_{\rm Ly\alpha}$ value consistent with an ionized IGM and associate deviations below this value with evolution in the IGM ionization state in a similar manner as above. Following this approach, the lack of Lyα in the Richard et al. (2008) sample and Kneib et al. (2004) source

suggests a decrement of >1.9 times which in turn would suggest a neutral fraction of $x_{\rm H\,I} > 0.3$ at $z \simeq 7.3$.

With new ground-based surveys (e.g. UltraVISTA) and WFC3 programs set to reveal hundreds of z and Y drops in the next several years, it should be possible to derive accurate Lyα fractions over the redshift range $6 \lesssim z \lesssim 8$. Indeed, we estimate that feasible campaigns with optical and near-IR multi-object spectrographs should easily be able to detect Lyα equivalent widths as low as 30–50 Å (rest-frame) for a sample of 200 z- and Y-band dropouts with continuum magnitudes spanning $26 \lesssim m \lesssim 28$, enabling much improved statistics on the fraction of LBGs with Lyα emission and the possibility to measure Lyα fractions as low as $\simeq$1 per cent. With such a spectroscopic sample, it will be easy to identify whether the Lyα fraction at $6.5 \lesssim z \lesssim 8$ shows a deficit with respect to measurements at $z \simeq 5$–6. In fact, this data set would enable the characterization of Lyα fractions more than 10 times lower than those expected at $z \simeq 7$ in the absence of any change in the IGM ionization state (Fig. 15). With these results, it should be trivial to identify the differential evolution in the Lyα fraction that would be expected from reionization; in the context of the simulations of McQuinn et al. (2007), these results enable the IGM ionization state to be tracked between fully ionized ($x_{\rm H\,I} \simeq 0.0$) and almost completely neutral ($x_{\rm H\,I} \simeq 0.8$).

6 SUMMARY AND CONCLUSIONS

In this paper, we have presented a new technique aimed at constraining reionization. By measuring the luminosity-dependent fraction of continuum dropouts with strong Lyα emission at $z \simeq 4, 5, 6, 7$ and so on, we are sensitive to sudden changes in the transmission of Lyα photons that would be expected if the ionization state of the IGM changes, complementary to past efforts to link evolution in the Lyα LF to reionization (e.g. Malhotra & Rhoads 2004; Kashikawa et al. 2006; Iye et al. 2006; Ota et al. 2008). The spectra not only provide information on Lyα but also reveal constraints on the absorbing gas along the line of sight and provide a robust spectroscopic sample for derivation of stellar populations (e.g. stellar masses, ages). Through this information, we seek to simultaneously provide insight into the evolution of the most important factors governing Lyα transmission (dust obscuration, H I covering fraction and kinematics), and to thereby better isolate the impact of the IGM ionization state on the evolving Lyα fraction.

To complete this Lyα fraction test, we have conducted a large Keck/DEIMOS spectroscopic survey of dropouts in the GOODS-S and GOODS-N fields. The current Keck/DEIMOS sample includes 268 B drops, 95 V drops, 64 i' drops and 17 z drops and uniquely extends to faint continuum magnitudes ($M_{\rm UV} \simeq -18$). When combined with existing VLT/FORS2 spectroscopic observations of B, V and i' drops in the two GOODS fields, our sample contains 627 dropouts. We summarize our key findings below.

(1) We present tentative spectroscopic identification of a z drop identified in the GOODS ERS imaging CDF-S (Wilkins et al. 2010a). The galaxy shows a 7σ emission feature at $z = 6.44$, consistent with the photometric redshift expected from the broad-band imaging. If confirmed, this would be the first WFC3 z drop with spectroscopic identification in the literature. Future deep spectroscopic study of WFC3 dropouts should vastly increase the number of LAEs in this redshift regime.

(2) The prevalence of LAEs is greater among low-luminosity galaxies. We find that the fraction of dropouts with Lyα equivalent widths in excess of 50 Å increases from $x_{\rm Ly\alpha} = 0.08 \pm 0.02$ at $M_{\rm UV} \simeq -21.0$ to $x_{\rm Ly\alpha} = 0.47 \pm 0.16$ for sources at $M_{\rm UV} \simeq -19.0$. This result is consistent with previous studies comparing the UV and Lyα LF for samples of narrowband LAEs (Ouchi et al. 2008). This finding demonstrates that a large fraction of galaxies at the faint-end of dropout samples are likely very similar to the high-EW and UV-faint LAEs found via narrowband filters.

(3) We find that the fraction of strong LAEs at fixed luminosity moderately increases towards earlier time in the redshift range $3 \lesssim z \lesssim 6$. Binning our sample in two redshift ranges ($3.0 < z < 4.5$) and ($4.5 < z < 6.0$), we find that the fraction of LAEs with rest-frame equivalent width in excess of 50 Å increases in each luminosity bin considered ($\mathrm{d}x_{\rm Ly\alpha}/\mathrm{d}z = 0.05 \pm 0.03$).

(4) We examined the possibility that these luminosity and redshift-dependent trends are driven by evolution in the dust obscuration of high-redshift galaxies. We find that the $z \simeq 4$ sources with strong Lyα emission have considerably bluer UV slopes, implying significantly less dust extinction. This result is consistent with a range of observational studies (e.g. Shapley et al. 2003; Pentericci et al. 2009; Kornei et al. 2010). In light of recent results revealing that dust obscuration decreases toward lower luminosities and higher redshifts (Reddy & Steidel 2009; Bouwens et al. 2009b), it appears that dust evolution plays a major role in governing the Lyα fraction.

(5) We discuss the possibility that the covering fraction of hydrogen may be lower in low-luminosity galaxies. In more luminous galaxies, strong Lyα emission is generally coupled with low dust extinction and low equivalent width ISM absorption lines (Shapley et al. 2003), the latter of which appears to arise from a non-uniform covering fraction of neutral hydrogen (Quider et al. 2009). Given the increased prevalence of strong LAEs and low dust obscuration at low luminosity, this result may suggest that galaxies with a non-uniform covering fraction may be much more common among UV-faint systems. Strong LAEs with UV faint continua do appear to show weak low-ionization ISM absorption (Stark et al. 2010, in preparation), but higher S/N and higher resolution spectra of gravitationally lensed galaxies are required to directly measure the covering fraction. We note that if the covering fraction of hydrogen is indeed lower for low-luminosity galaxies, this would in turn imply that Lyman continuum photons may more easily escape from feeble galaxies, a trend that appears to be seen in $z \simeq 3$ galaxies with deep Keck spectra (Steidel et al. 2010, in preparation).

(6) We have measured the fraction of z drops with strong Lyα emission in our spectroscopic sample, enabling us to constrain $x_{\rm Ly\alpha}$ at $z \simeq 6.5$. The estimated Lyα fraction appears consistent with the redshift trend seen over $3 \lesssim z \lesssim 6$. However the current sample is far too small to rule out a decline to $z \simeq 6.5$. Efforts to extend these studies to $z \simeq 7$ have thus far failed to locate Lyα emission. The lack of strong Lyα in the Keck spectra of seven candidate LBGs in Richard et al. (2008) and the lensed $z \simeq 6.8$ source in Kneib et al. (2004) provides tantalizing evidence that the Lyα fraction declines by $z \simeq 7$. The availability of more robust WFC3/IR $z \simeq 7$ samples (e.g. Oesch et al. 2010; McLure et al. 2010; Bunker et al. 2010) enables this possibility to be readily tested with the new generation of near-infrared multi-object spectrographs.

(7) Using recent simulations linking the evolution in the abundance of LAEs to the IGM ionization state (McQuinn et al. 2007), we examine the possibility of placing constraints on reionization with our spectroscopic sample. While we emphasize that the results are strongly model-dependent, if the evolution in the Lyα fraction at $z \simeq 7$ were to hold up (>1.9 times decline with respect to the value predicted from extrapolating $4 < z < 6$ trends), the McQuinn et al. (2007) simulations would suggest that the neutral fraction of the

IGM is $x_{\rm HI} \gtrsim 0.3$ at $z \simeq 7$. More robust estimates of the $z \simeq 6.5$–7 Lyα fractions are needed to confirm these preliminary findings.

The recent emergence of new photometric samples of dropouts at $z \gtrsim 7$ with the WFC3 onboard *HST* provides a great deal of promise for extending this test in the future. Long exposures with upcoming near-infrared multi-object spectrographs will enable significant detections of strong Lyα emission lines from sources as faint as $J \simeq 28$, allowing the Lyα fraction test to be extended to $z \simeq 8$.

ACKNOWLEDGMENTS

DPS acknowledges financial support from a postdoctoral fellowship from the Science Technology and Research Council and a Schlumberger Interdisciplinary Research Fellow at Darwin College. RSE acknowledges financial support from the Royal Society. We thank our referee, Simon Morris, for very thoughtful comments which improved the quality of the paper. We acknowledge useful conversations with George Becker, Jim Dunlop, Anna Quider, Ross McLure, Johan Richard, Elizabeth Stanway and Stephen Wilkins, and we thank Sebastiano Cantalupo for comments after reading an earlier version of the manuscript.

REFERENCES

Ando M., Ohta K., Iwata I., Akiyama M., Aoki K., Tamura N., 2006, ApJ, 645, L9
Ando M., Ohta K., Iwata I., Akiyama M., Aoki K., Tamura N., 2007, PASJ, 59, 717
Atek H., Kunth D., Hayes M., Östlin G., Mas-Hesse J. M., 2008, A&A, 488, 491
Balestra I. et al., 2010, A&A, 512, 12
Becker G. D., Rauch M., Sargent W. L. W., 2007, ApJ, 662, 72
Benítez N., 2000, ApJ, 536, 571
Bertin E., Arnouts S., 1996, A&AS, 117, 393
Bouwens R. J., Illingworth G. D., Blakeslee J. P., Franx M., 2006, ApJ, 653, 53
Bouwens R. J., Illingworth G. D., Franx M., Ford H., 2007, ApJ, 670, 928
Bouwens R. J. et al., 2009a, ApJ, 690, 1764
Bouwens R. J. et al., 2009b, ApJ, 705, 936
Bouwens R. J. et al., 2010a, ApJ, 709, L133
Bouwens R. J. et al., 2010b, ApJ, 708, L69
Bunker A. J., Stanway E. R., Ellis R. S., McMahon R. G., McCarthy P. J., 2003, MNRAS, 342, L47
Bunker A. J., Stanway E. R., Ellis R. S., McMahon R. G., 2004, MNRAS, 355, 374
Bunker A. et al., 2010, MNRAS, submitted (arXiv:0909.2255)
Charlot S., Fall S. M., 1993, ApJ, 415, 580
Coe D., Benítez N., Sánchez S. F., Jee M., Bouwens R., Ford H., 2006, AJ, 132, 926
Davé R., 2008, MNRAS, 385, 147
Davis M. et al., 2003, in Guhathakurta P., ed., SPIE Conf. Proc. Vol. 4834, Discoveries and Research Prospects from 6- to 10-Meter-Class Telescopes II. SPIE, Bellingham, p. 161
Dayal P., Maselli A., Ferrara A., 2010, MNRAS, submitted (arXiv/1002.0839)
Dijkstra M., Lidz A., Wyithe J. S. B., 2007a, MNRAS, 377, 1175
Dijkstra M., Wyithe J. S. B., Haiman Z., 2007b, MNRAS, 379, 253
Dow-Hygelund C. C. et al., 2007, ApJ, 660, 47
Dunkley J. et al., 2009, ApJS, 180, 306
Egami E. et al., 2005, ApJ, 618, L5
Eyles L. P., Bunker A. J., Stanway E. R., Lacy M., Ellis R. S., Doherty M., 2005, MNRAS, 364, 443
Eyles L. P., Bunker A. J., Ellis R. S., Lacy M., Stanway E. R., Stark D. P., Chiu K., 2007, MNRAS, 374, 910
Faber S. M. et al., 2003, in Iye M., Moorwood A. F. M., eds, SPIE Conf. Proc. Vol. 4841, Instrument Design and Performance for Optical/Infrared Grand-based Telescopes. SPIE, Bellingham, p. 1657
Fan X. et al., 2006, AJ, 132, 117
Filippenko A. V., 1982, PASP, 94, 715
Finkelstein S. L., Rhoads J. E., Malhotra S., Grogin N., Wang J., 2008, ApJ, 678, 655
Furlanetto S. R., Zaldarriaga M., Hernquist L., 2006, MNRAS, 365, 1012
Giavalisco M. et al., 2004a, ApJ, 600, L103
Giavalisco M. et al., 2004b, ApJ, 600, L93
González V., Labbé I., Bouwens R. J., Illingworth G., Franx M., Kriek M., Brammer G. B., 2010, ApJ, 713, 115
Haiman Z., Spaans M., 1999, ApJ, 518, 138
Hansen M., Oh S. P., 2006, MNRAS, 367, 979
Hayes M. et al., 2010, Nat, 464, 562
Hibon P. et al., 2010, A&A, 515, 97
Iliev I. T., Shapiro P. R., McDonald P., Mellema G., Pen U., 2008, MNRAS, 391, 63
Iye M. et al., 2006, Nat, 443, 186
Kashikawa N. et al., 2006, ApJ, 648, 7
Kneib J.-P., Ellis R. S., Santos M. R., Richard J., 2004, ApJ, 607, 697
Kornei K. A., Shapley A. E., Erb D. K., Steidel C. C., Reddy N. A., Pettini M., Bogosavljević M., 2010, ApJ, 711, 693
Labbé I. et al., 2010, ApJ, 708, 26
Larson D. et al., 2010, ApJ, submitted (arXiv:1001.4635)
Leitherer C. et al., 1999, ApJS, 123, 3
MacArthur L. A., Ellis R. S., Treu T., U V., Bundy K., Moran S., 2008, ApJ, 680, 70
McLean I. S. et al., 1998, in Fowler A. M., ed., SPIE Conf. Proc. Vol. 3354, Infrared Astronomical Instrumentation. SPIE, Bellingham, p. 566
McLure R. J., Dunlop J. S., Cirasuolo M., Koekemoer A. M., Sabbi E., Stark D. P., Targett T. A., Ellis R. S., 2010, MNRAS, 403, 960
McQuinn M., Hernquist L., Zaldarriaga M., Dutta S., 2007, MNRAS, 381, 75
Malhotra S., Rhoads J. E., 2002, ApJ, 565, L71
Malhotra S., Rhoads J. E., 2004, ApJ, 617, L5
Meiksin A., 2006, MNRAS, 365, 807
Mesinger A., Furlanetto S. R., 2008, MNRAS, 386, 1990
Meurer G. R., Heckman T. M., Calzetti D., 1999, ApJ, 521, 64
Neufeld D. A., 1991, ApJ, 370, L85
Nilsson K. K., Möller-Nilsson O., Møller P., Fynbo J. P. U., Shapley A. E., 2009, MNRAS, 400, 232
Oesch P. A. et al., 2010, ApJ, 709, L16
Oke J. B., Gunn J. E., 1983, ApJ, 266, 713
Ono Y. et al., 2010, MNRAS, 402, 1580
Ota K. et al., 2008, ApJ, 677, 12
Ouchi M. et al., 2004, ApJ, 611, 660
Ouchi M. et al., 2008, ApJS, 176, 301
Ouchi M. et al., 2009, ApJ, 706, 1136
Pentericci L., Grazian A., Fontana A., Castellano M., Giallongo E., Salimbeni S., Santini P., 2009, A&A, 494, 553
Pirzkal N., Malhotra S., Rhoads J. E., Xu C., 2007, ApJ, 667, 49
Quider A. M., Pettini M., Shapley A. E., Steidel C. C., 2009, MNRAS, 398, 1263
Quider A. M., Shapley A. E., Pettini M., Steidel C. C., Stark D. P., 2010, MNRAS, 402, 1467
Reddy N. A., Steidel C. C., 2009, ApJ, 692, 778
Rhoads J. E., Malhotra S., 2001, ApJ, 563, L5
Rhoads J. E. et al., 2009, ApJ, 697, 942
Richard J., Stark D. P., Ellis R. S., George M. R., Egami E., Kneib J., Smith G. P., 2008, ApJ, 685, 705
Salvadori S., Ferrara A., 2009, MNRAS, 395, L6
Santos M. R., 2004, MNRAS, 349, 1137
Schaerer D., 2003, A&A, 397, 527
Schaerer D., de Barros S., 2009, A&A, 502, 423
Schaerer D., Verhamme A., 2008, A&A, 480, 369

Shapley A. E., Steidel C. C., Adelberger K. L., Dickinson M., Giavalisco M., Pettini M., 2001, ApJ, 562, 95
Shapley A. E., Steidel C. C., Pettini M., Adelberger K. L., 2003, ApJ, 588, 65
Shapley A. E., Steidel C. C., Pettini M., Adelberger K. L., Erb D. K., 2006, ApJ, 651, 688
Shimasaku K. et al., 2006, PASJ, 58, 313
Stanway E. R., Bunker A. J., McMahon R. G., 2003, MNRAS, 342, 439
Stanway E. R., Bunker A. J., McMahon R. G., Ellis R. S., Treu T., McCarthy P. J., 2004, ApJ, 607, 704
Stanway E. R., McMahon R. G., Bunker A. J., 2005, MNRAS, 359, 1184
Stanway E. R. et al., 2007, MNRAS, 376, 727
Stanway E. R., Bremer M. N., Lehnert M. D., 2008, MNRAS, 385, 493
Stark D. P., Bunker A. J., Ellis R. S., Eyles L. P., Lacy M., 2007a, ApJ, 659, 84
Stark D. P., Ellis R. S., Richard J., Kneib J., Smith G. P., Santos M. R., 2007b, ApJ, 663, 10
Stark D. P., Ellis R. S., Bunker A., Bundy K., Targett T., Benson A., Lacy M., 2009, ApJ, 697, 1493
Steidel C. C., Adelberger K. L., Giavalisco M., Dickinson M., Pettini M., 1999, ApJ, 519, 1
Steidel C. C., Adelberger K. L., Shapley A. E., Pettini M., Dickinson M., Giavalisco M., 2000, ApJ, 532, 170
Steidel C. C., Adelberger K. L., Shapley A. E., Pettini M., Dickinson M., Giavalisco M., 2003, ApJ, 592, 728
Steidel C. C., Erb D. K., Shapley A. E., Pettini M., Reddy N., Bogosavljević M., Rudie G. C., Rakic O., 2010, ApJ, 717, 289
Vanzella E. et al., 2002, A&A, 396, 847
Vanzella E. et al., 2005, A&A, 434, 53
Vanzella E. et al., 2006, A&A, 454, 423
Vanzella E. et al., 2008, A&A, 478, 83
Vanzella E. et al., 2009, ApJ, 695, 1163
Verhamme A., Schaerer D., Atek H., Tapken C., 2008, A&A, 491, 89
Verhamme A., Schaerer D., Maselli A., 2006, A&A, 460, 397
Wilkins S. M., Bunker A. J., Ellis R. S., Stark D., Stanway E. R., Chiu K., Lorenzoni S., Jarvis M. J., 2010a, MNRAS, 403, 938
Wilkins S. M., Bunker A. J., Lorenzoni S., Caruana J. 2010b, MNRAS, in press (arXiv:1002.4866)
Yan H., Dickinson M., Giavalisco M., Stern D., Eisenhardt P. R. M., Ferguson H. C., 2006, ApJ, 651, 24
Yoshida M. et al., 2006, ApJ, 653, 988
Zheng Z., Cen R., Trac H., Miralda-Escudé J., 2010, ApJ, 716, 574

This paper has been typeset from a TEX/LATEX file prepared by the author.